Aust. Met. Mag. 56 (2007) 241-266

What is the trigger for tropical cyclogenesis?

David S. Nolan

Rosenstiel School of Marine and Atmospheric Science,
University of Miami, Miami, Florida, USA

(Manuscript received March 2007; revised August 2007)

The development of a tropical cyclone from a pre-existing, weak, warm-core vortex is investigated with high-resolution cloud-resolving simulations using the Weather Research and Forecast Model (WRF). The simulation design and initial conditions are quite favourable for tropical cyclogenesis: the environment has a tropical sounding with no mean wind or wind shear, and the sea-surface temperature is held constant at 29°C. Nonetheless, it is found that sporadic convection must occur for 48 to 72 hours before genesis and rapid intensification begins.

During this time, before intensification, the vortex is found to go through important structural changes in both its wind field and its thermodynamics. While the low-level wind field decays due to friction, the inner core slowly becomes humidified due to moist detrainment and precipitation from deep convective towers. As the relative humidity in the core exceeds values of 80 per cent over most of the depth of the troposphere, a mid-level vortex forms, contracts and intensifies. Once the mid-level vortex has reached a sufficient strength, and the inner core is nearly saturated, a smaller scale vortex forms very rapidly at the surface. This smaller vortex becomes the core of an intensifying tropical cyclone.

This process is explored through careful study of the inner-core dynamics and thermodynamics, with close attention paid to the changes in the moist convection as the inner core approaches saturation. While the frequency of deeper and stronger updraughts increases with time, the frequency of cool downdraughts remains essentially unchanged. In the hours before genesis, the intensification of the mid-level vortex leads to a large increase in the efficiency of the conversion of latent heat energy to the kinetic energy of the cyclonic wind field. The relative importances of the mid-level vortex and inner-core saturation are illustrated with additional simulations with different initial conditions and environmental soundings. Implications of these results for identifying and forecasting tropical cyclogenesis are discussed.

Introduction

Background

In their recent review of tropical cyclones in the Australian region, Dare and Davidson (2004) pointed out that a large fraction of these cyclones are formed rather close to land. In optimal conditions, tropical cyclones can form and then strengthen to significant intensity in as little as three days time. Along with the fact that cyclones in this region do not consistently follow any characteristic paths, this enhances the forecasting challenge for Australian meteorologists. The very recent case of tropical cyclone (TC) *Larry* (2006) is just such an example: the cyclone that became *Larry* was first monitored at 10 am on 16

Corresponding author address: Prof. David S. Nolan, RSMAS/MPO, 4600 Rickenbacker Causeway, Miami, FL 33149, USA.
Email: dnolan@rsmas.miami.edu

March, achieved (Australian) category 1 status as a named cyclone just 42 hours later, and was approaching the coast as a severe category 4 cyclone after just another 24 hours (Australian Bureau of Meteorology 2007). In this example, neither a five-day nor even a four-day forecast of the TC landfall was possible without some anticipation of the genesis of the storm. Thus, the inability to accurately forecast TC genesis can be a critical barrier to achieving sufficiently long warning times for landfalling cyclones.

The challenge of understanding tropical cyclogenesis has been an area of great interest in tropical meteorology for over 50 years. The earliest investigators recognised the critical role that deep, moist, convective updraughts must play in overcoming the inhibition to organised vertical motion caused by the static stability of the atmosphere, even in the tropics (Malkus and Riehl 1960; Riehl and Malkus 1961; Gray 1968). Theories to explain the feedback between deep convection and the surrounding large-scale motions were developed that described TC genesis as a fundamental instability of the tropical atmosphere to small perturbations (Charney and Eliassen 1964; Ooyama 1964). These ideas were ultimately found to be inconsistent with the observation that only a small fraction of seemingly appropriate tropical disturbances make the transition to a tropical cyclone. In the last 25 years, the widely held view has evolved to the idea that TC genesis can be thought of as a 'finite-amplitude' instability, in that a pre-existing disturbance of some strength, such as an easterly wave, monsoon depression, or even a baroclinic cyclone, is required for genesis (McBride 1981; McBride and Zehr 1981; Frank 1987; Rotunno and Emanuel 1987; Emanuel 1989).

With the understanding that genesis requires a pre-existing disturbance of sufficient amplitude, the natural question has turned to how such a 'sufficient' disturbance forms in the first place, and how to differentiate between the many 'sufficient-appearing' disturbances that do and do not become tropical cyclones. In recent years, a number of papers have proposed that the merger and/or axisymmetrisation of pre-existing vortices is a possible, and perhaps necessary, step in this process. The generation and enhancement of mid-level vertical vorticity by stratiform precipitation in mesoscale convective systems (MCSs) was illustrated in studies by Raymond and Jiang (1990), Chen and Frank (1993) and Fritsch et al. (1994). Based on observations of TC genesis in the Pacific, Ritchie and Holland (1997) and Simpson et al. (1997) proposed that the formation and then merger of mesoscale, mid-level vortices generated by convective complexes, with scales of 100 to 200 km, can lead to a single mesoscale convective vortex that may then develop into a tropical cyclone. An additional element of their arguments was that the merger of mid-level, mesoscale vortices leads to a greater penetration depth of the circulation, increasing the low-level vorticity.

Davis and Bosart (2001) reported that a similar process was at work, mostly on smaller scales (perhaps 20-40 km), in a mesoscale model simulation of the formation of hurricane *Diana* (1984). As computing power and observational technologies have allowed for both the simulation and observation of smaller and smaller scales, the vortex merger concept has focused more closely on much smaller vortices associated with individual convective events or even individual updraughts. When the grid spacing of the *Diana* simulation was decreased from 9 to 3 km, Davis and Bosart (2002) and Hendricks et al. (2004) found a close correlation between convective updraughts and vertical vorticity anomalies, and that the mesoscale vortex that later developed into the primary circulation appeared to develop from, at least in part, the interactions and merger of the positive vorticity anomalies. Hendricks et al. introduced the notion of 'vortical hot towers' (VHTs) which are strong cumulus updraughts that generate strong vorticity anomalies of both positive and negative sign. They proposed that VHTs have an important and possibly necessary role in TC genesis, by generating the larger-valued positive vorticity anomalies that then organise and coalesce into the smaller scale (as compared to the surrounding mesoscale), stronger vortex that eventually becomes the core of a developing cyclone. They also proposed that the process of 'diabatic vortex merger' was important, whereby interacting, like-signed vortices initiate new convective updraughts that then accelerate the merger process.

Observational evidence for the existence and interactions of VHTs in developing cyclones was provided by Reasor et al. (2005) through analysis of airborne Doppler radar observations and by Sippel et al. (2006) through analysis of surface-based Doppler radar. Montgomery et al. (2006) continued investigation of the VHT hypothesis with highly idealised numerical simulations of TC genesis from a pre-defined axisymmetric vortex on the f-plane, providing additional examples of VHTs and their merger, and showing that a significant fraction of the vertical vorticity in the VHTs comes from tilting of the ambient horizontal vorticity. They did find, however, that the dominant forcing for the secondary circulation that drives the overall vortex intensification was the latent heat release in convection, with only a small contribution from 'eddy flux' terms related to asymmetric vortex interactions and merger.

An alternative, though not necessarily exclusive, point of view of TC genesis emphasises the moist thermodynamics of the precursor, mesoscale vortex.

Based on observations of the genesis of hurricane *Guillermo*, Bister and Emanuel (1997) proposed that the key process leading to genesis was the saturation and cooling of the lower and middle levels of the mesoscale convective vortex by precipitation and evaporative cooling. While also a necessary consequence of maintaining thermal wind balance as the mid-level vortex strengthens, lowering the temperature in the middle and lower levels serves two additional purposes toward TC genesis: it brings the lower atmosphere closer to saturation, and it destabilises the lower atmosphere to moist convection from the boundary layer after it has recovered from the cooling and low-level divergence driven by the stratiform precipitation. Bister and Emanuel proposed that this recovery period is followed by an eruption of deep convection from the surface. Due to the increased low and mid-level humidity, this new convection is associated with weaker downdraughts and cooling, and thus causes low-level convergence and vortex intensification. As the low-level circulation strengthens, the wind-induced surface heat exchange (WISHE) feedback will take over, leading to steady or rapid intensification of the cyclone.

In a study of the same storm and two others in the same region, Raymond et al. (1998) also found that vorticity was maximised in the middle levels before genesis, and that genesis was preceded by an increase in mid-level humidity and a decrease in the fraction of downdraught mass flux.

Tory et al. (2006a), (2006b) documented several cases of TC genesis in the Australian region as simulated with a mesoscale model specifically designed for TC forecasting. Despite the much lower resolution of that model (about 15 km), they too saw VHT-like formation and merger leading to the formation of the dominant vortex that became the TC core. However, the large horizontal resolution and the use of a convective parametrisation scheme may have prevented the generation of regions of mixed stratiform and deep convection (Houze 1997), perhaps biasing the dynamics toward convective updraughts, low-level convergence, and low-level vertical vorticity generation in the earlier stages. Furthermore, since VHT interactions were present in both developing and non-developing cases, Tory et al. (2007) determined that the larger-scale vortex intensification by adjustment to deep convective heating was the more critical process, consistent with the results of Montgomery et al. (2006) that the primary forcing for the mean vortex development was the mean diabatic heating.

One way to overcome the limitations and uncertainties of using convective parametrisations is to use a 'cloud-resolving' model with resolutions of 4 km or less. While the resolutions used by Hendricks et al. (2004) and Montgomery et al. (2006) were certainly of this category, they focused almost entirely on the vortex dynamics, and did not document the evolution of the broader precipitation and convection embedded in their developing cyclones. As we shall see in this study, an evolution quite similar to that described by Bister and Emanuel (1997) can occur in a high-resolution, full-physics, cloud-resolving simulation of TC genesis.

Preliminary results and motivation

The motivation for this study came from some interesting results of idealised numerical simulations quite similar in design to those of Montgomery et al. (2006). While the details of the model, domain, and parametrisations will be described shortly, it suffices for the moment to say that the simulation depicts the formation of a tropical cyclone from an initially axisymmetric vortex with maximum cyclonic winds of 10 m s^{-1} that are maximum at the surface at a radius of 100 km, and monotonically decreasing upward into the middle and upper troposphere. A cross-section of the initial vortex is shown in Fig. 1(a). This initial wind field is quite unrealistic, but as we will show later, it serves to emphasise the structural changes that occur in the evolution toward TC genesis. The lower boundary condition is an ocean with sea-surface temperature (SST) fixed at 29°C, the environment is at rest with no mean wind or wind shear, and the background environment is that of the Jordan Mean Hurricane Season sounding for the Caribbean (Jordan 1958).

Such an environment would seem ideal for rapid development of a pre-existing, low-level vortex into a tropical cyclone. However, rather than intensifying, the intensity of the simulated vortex (as indicated by the standard measures of maximum 10 m wind speed and minimum surface pressure) remains nearly constant for 60 hours, as shown in Fig. 1(b). The noisy oscillations in the 10 m wind speed are due to local convective downdraughts and gusts. After 60 hours, the vortex begins a sudden and rapid increase in intensity, becoming a hurricane in just about 36 hours. The suddenness of this transition from a non-developing to a developing cyclone is further emphasised in Fig. 1(c), which shows the same data but at hourly intervals from t = 36 to 72 hours. The negative pressure anomaly is almost perfectly flat until t = 61 hours, after which it begins a distinct increase. An equally evident increase in surface wind (which might not even be measurable with today's observing systems) does not occur until six hours later. The sharp transition from a non-intensifying to an intensifying cyclone naturally begs the question as to what changes in the system 'triggered' the sudden development.

Fig. 1 Initial wind field and intensity evolution for the control simulation: (a) north-south vertical cross-section of the initial zonal wind; (b) maximum 10 m wind speed and negative pressure anomaly every six hours; (c) the same, but for one-hour intervals from *t* = 36 to 72 hours.

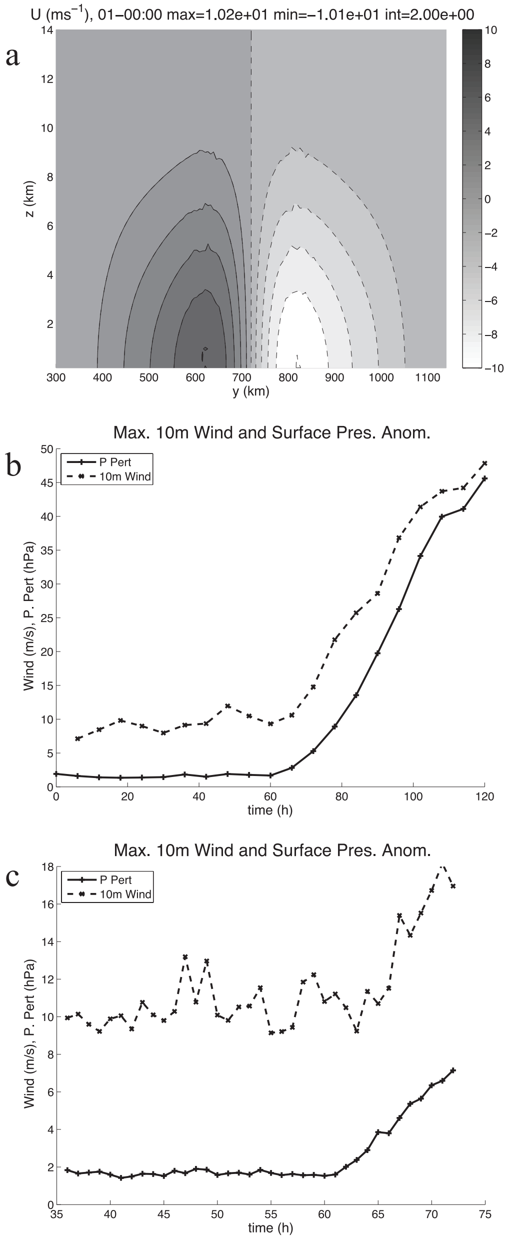

Undoubtedly, the first 6-12 hours of the delayed development is due to the necessary time for development of free convection from the balanced initial state. This delay or 'incubation time' before intensification of a tropical cyclone in favourable conditions has been reported before in axisymmetric simulations with both parametrised and resolved convection (Ooyama 1969; Rotunno and Emanuel 1987; Emanuel 1989; Bister and Emanuel 1997), although most of those simulations did not show the same suddenness in the transition. The present simulation (and those like it in the recent literature), with 2 km horizontal resolution, offers the chance to study this transition in a fully three-dimensional model that resolves updraughts, downdraughts, and the vorticity anomalies they generate.

We shall see below that although the surface winds and minimum pressure are nearly constant for the first 2.5 days of the simulation, during this time the vortex is changing significantly in both its kinematic and thermodynamic structures. We find that these changes lead to, and are necessary for, the formation of a smaller-scale, low-level vortex which becomes the tropical cyclone. The goal of this paper is to document and try to understand the changes that lead to tropical cyclogenesis from a weak vortex. In particular, we will try to determine if there are any structural or thermodynamic changes that distinctly precede or trigger cyclogenesis, in the hope that such changes might be observable in the future.

We first present the numerical model, parametrisations and initial conditions used for the simulations in this study, followed by a detailed description of the results of the simulation depicted in Fig. 1, and of a number of analysis tools that we will use to diagnose the cyclogenesis process. We then present the results of a number of additional simulations with variations in vortex structure and background humidity profiles followed by further analyses of the genesis process. Finally, some conclusions and implications of this work are discussed.

Model, domain and initial conditions

Numerical model

The atmospheric model used for this study was version 2.1.1 of the Weather Research and Forecast Model (WRF). WRF is a fully compressible model of the atmosphere designed for mesoscale and convective-scale simulations of real-case and idealised weather phenomena (Skamarock et al. 2005). WRF uses high-order advection schemes on an Arakawa-C grid, with $\eta = p_h/p_{hs}$ as a terrain-following vertical coordinate (although there is no terrain in the simulations presented here), where p_h and p_{hs} are the hydrostatic pressure and the hydrostatic surface pressures, respectively (Laprise 1992). The time integration uses 3rd order Runge-Kutta time stepping (Wicker and Skamarock 2002).

All simulations use a single high-resolution grid embedded inside a larger, lower-resolution grid, with full two-way interactive coupling (nesting) between them. The outer grid has 240x240 points with 6 km horizontal grid spacing in the *x* and *y* directions. The inner grid has 180x180 points with 2 km grid spacing. The boundary conditions on the outer grid are doubly periodic. The size of the outer grid would be undoubtedly too small to simulate the complete life cycle of a tropical cyclone, but we found it adequate for the simulation of the early development and genesis process. The vertical discretisation uses 40 levels equally spaced in the η coordinates, thus being stretched in height, with 10 levels in the lowest 2.0 km. The model top is defined by pressure but sits at approximately 18 km altitude. The advective time step was 20 s on both grids, with six acoustic steps for each advective step.

Parametrisations for unresolved physical processes that were available with WRF 2.1.1 were used, all of which are closely related to commonly used schemes for research and numerical weather prediction. Convection is resolved explicitly and there is no cumulus parametrisation. For microphysics, the WRF Single-Moment (WSM) 6-class scheme (with graupel) is used (Hong et al. 2004). For the planetary boundary layer, we use the Yonsei University (YSU) scheme (Noh et al. 2003), which is an advancement of the Medium Range Forecast (MRF) scheme of Hong et al. (1996). No long-wave or short-wave radiation was included in the simulations.*

The model uses a Smagorinsky-type resolution-dependent horizontal diffusion, with vertical diffusion in the boundary layer determined by the PBL scheme, and determined by shear and the Richardson number in the free atmosphere. An upper-level Rayleigh damping zone diminishes gravity waves and convection that penetrate above 15 km altitude.

Initial conditions

Each simulation is initialised with an axisymmetric wind field *V(r, z)* that is constructed as follows. An azimuthal wind profile is first computed from radial integration of a vertical vorticity profile

$$v_0(r) = \frac{1}{r}\int_0^r r\zeta\, dr \qquad \text{...1}$$

where ζ is the relative vertical vorticity that is defined as a Gaussian function of radius,

$$\zeta(r) = A \exp\left\{-\left(\frac{r}{b}\right)^2\right\} \qquad \text{...2}$$

Since the total circulation must be zero in a doubly periodic domain, the velocity profile is forced to go smoothly to zero across some radius R as:

$$v_s(r) = v_0(r) \times \exp\left\{-\left(\frac{r}{R}\right)^6\right\} \qquad \text{...3}$$

Finally, the wind profile is extended into the vertical with the following form:

$$V(r,z) = v_s(r) \times \exp\left\{-\frac{|z - z_{\max}|^{\alpha}}{\alpha L_z^{\alpha}}\right\} \qquad \text{...4}$$

where L_z indicates the depth of the approximately barotropic part of the vortex, α is the decay rate with height above and below the barotropic zone, and $z_{\max}$ is the altitude of the maximum cyclonic wind speed. For most of the simulations, the parameters A and b are chosen to define a vortex with a radius of maximum winds (RMW) = 100 km and maximum initial cyclonic wind speed $v_{\max}$ = 10 m s^{-1}. For the initial vortex described in the introduction, these maximum winds are set at the surface, i.e., $z_{\max}$ = 0, and the other parameters are set to L_z = 5000.0 m and α = 2.0. This initial condition shall be referred to as the 'surface vortex case' and is illustrated in Fig. 1(a).

For all vortices, the initial wind field is smoothed to zero across R = 350 km as in Eqn 3. The pressure and temperature fields that hold the initial axisymmetric wind field in hydrostatic and gradient wind balance are computed with the iterative procedure of Nolan et al. (2001). To initiate random convection, random noise with zero mean and variance 0.1 m s^{-1} is added to the zonal (u) and meridional (v) wind fields in the annulus 70 km$<r<$130 km ; this noisiness can be seen in the contours of u in Fig. 1(a) and in subsequent figures. All simulations use a constant Coriolis parameter of f = 5.0x10^{-5} s^{-1}, corresponding to – with apologies to our friends in the southern hemisphere – a latitude of 20°N.

Results

The surface vortex case

Returning to the example of TC genesis from the surface vortex case as described in the introduction, we examine the evolution of the vortex leading up to the time of rapid development at t = 61 hours. As mentioned above, the first 12 hours have little convective activity, due to the time required for conditional instability to develop from the frictional convergence and

* At the suggestions of two reviewers, we performed one simulation with standard short-wave and long-wave radiation schemes activated in the model. This led to a rapid cooling of the environment by as much as 2 K in the upper troposphere in the first 24 hours. In the real tropical atmosphere, a relatively constant sounding is maintained by a three-way balance between radiation, advection, and deep convection. Since the latter two forcings are not present at the start of the simulation, this leads to a rapid cooling which biases the simulation toward instability and cyclonic development.

random noise embedded in the initial conditions. Figure 2 shows vertical, north-south cross-sections of zonal velocity (u) and relative humidity (RH) at $t = 24, 48$ and 60 hours. The noisiness of the fields is due to the deep but intermittent convection occurring in and around the core of the vortex. At 24 hours, the 10 m s^{-1} maximum winds at the surface have decayed, and the lesser existing maxima are now at $z = 1.5$ km. The relative humidity shows that much of the middle and upper atmosphere is still relatively dry, with a few obvious plumes of near-saturation (RH > 90%) penetrating upward to heights of 10-12 km.

At 48 hours, the wind speeds are only slightly greater, and there is a notable upward displacement and deepening of the stronger winds, but there is no notable contraction of the vortex wind field. The RH

Fig. 2 **Vertical, north-south cross-sections through the centre of the vortex for the surface vortex case, at $t = 24, 48$ and 60 hours in the simulation, for zonal velocity (left) and relative humidity (right). Note in these and all subsequent figures, the dates and times in the title refer to the time from a start date of day 1, hour 0. The figures show the entirety of the inner grid with 2 km resolution. Negative contours are dashed.**

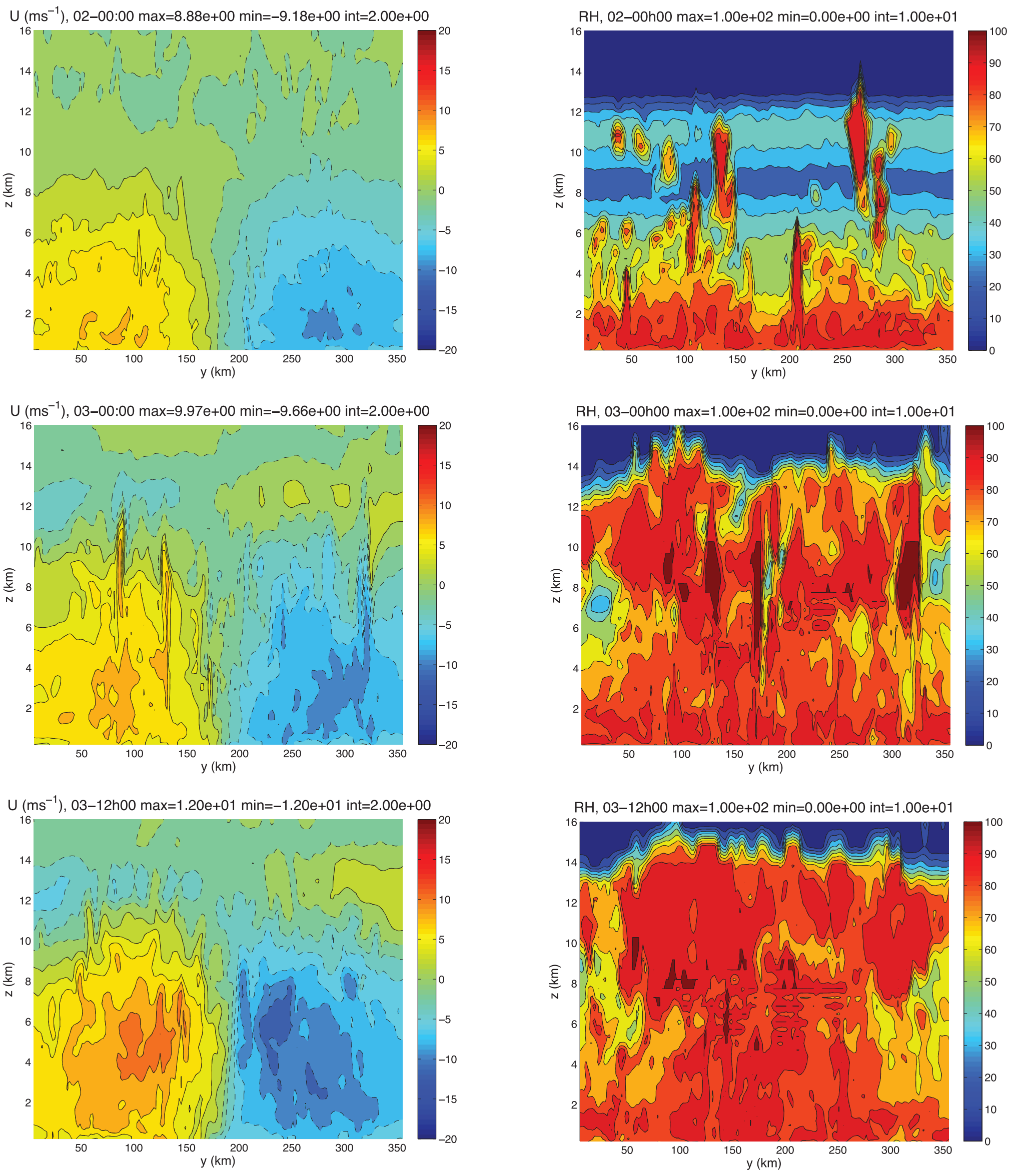

field, however, is substantially enhanced, with RH values above 80% predominant from the surface up to z = 12 km. Thus, the obvious change in this 24-hour period is the increase of humidity in the middle and upper levels in the core of the cyclone.

The wind field shows a significant change in the next 12 hours. The maximum u velocities have increased to 12 m s^{-1}, but more importantly, the maximum winds have risen to around z = 6 km and inward to within 60 km of the vortex centre (the centre is at y = 180 km in these figures). The RH field shows that the atmosphere has become nearly saturated throughout the core and out to over 100 km north and south of the centre.

A clearer view of the evolution of the vortex before 'genesis' and rapid intensification can be seen from azimuthally averaged azimuthal wind fields at t = 48, 54, 60 and 66 h, as shown in the first four panels of Fig. 3. Between 48 and 54 hours, there is a clear increase in

Fig. 3 Azimuthally averaged azimuthal winds around the centre of the developing cyclone for the surface vortex case: (a) t = 48 h; (b) t = 54 h; (c) t = 60 h; (d) t = 66 h; (e) t = 78 h; (f) t = 96 h. Zero contour is thickened, and dashed contours indicate negative values; note contour intervals and shading ranges are larger for (e) and (f).

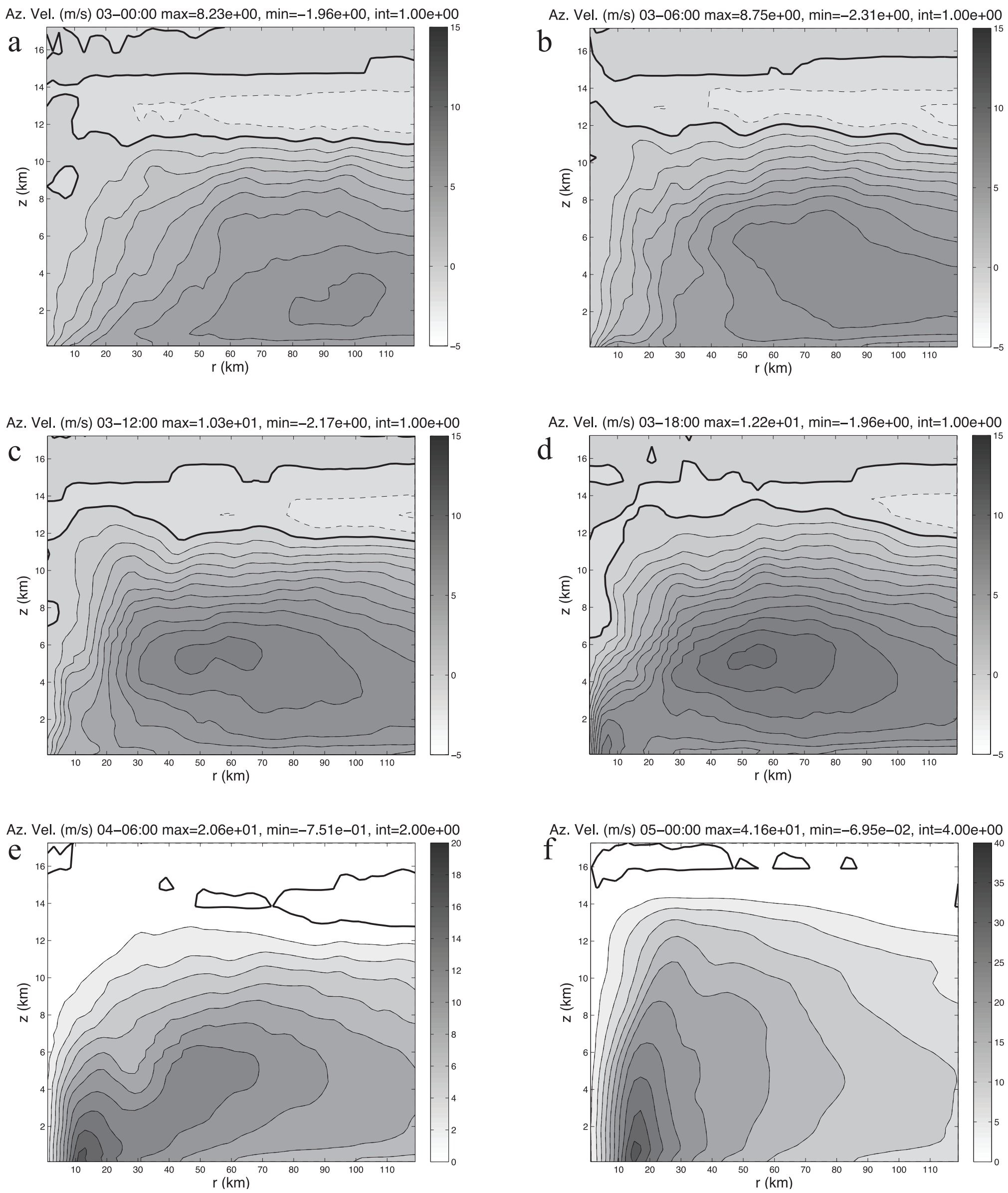

the altitude and the depth of the azimuthal wind. In the next six hours, the wind maximum intensifies and moves radially inward. Six hours later (t = 66 h), an amazingly small vortex has appeared at the surface, with azimuthally averaged wind speeds over 10 m s^{-1}.

In this and all the subsequent simulations, the appearance of this smaller scale, low-level vortex is closely correlated with an increase in the rate of pressure fall and substantial increases in deep convection near the vortex centre. In each case, we saw that rapid intensification (due to the very favourable environment with no shear) proceeded immediately after formation of this smaller vortex, and it is this vortex that grows and intensifies into the primary circulation. This can be seen in the last two panels of Fig. 3, which show the azimuthally averaged wind 12 and 30 hours after the formation of the smaller vortex (t = 78 and 96 h; note different contour intervals and shading for these plots). The mid-level wind maximum is superceded as the low-level vortex strengthens and expands. Since the formation of the low-level vortex so clearly marks the time when intensification begins, we use this moment to define the time of TC genesis. For the surface vortex case, the smaller-scale maximum in the low-level circulation first appears at t = 63 h (not shown).

Returning to the evolution leading up to genesis, the thermodynamically significant change that preceded the elevation and then contraction of the vortex wind field was the steadily increasing humidity in the core, with RH reaching values of 80 per cent or greater through most of the depth of the vortex. This is shown more succinctly in Fig. 4, which shows line plots of the mean value of the RH at various altitudes* averaged over a 160 km x 160 km box centred at the vortex centre, thus encompassing most of the region inside the original RMW. (In all calculations, the vortex centre was defined by the location of the minimum surface pressure after the surface pressure was smoothed 20 times by a 1-2-1 filter in both the x and y directions.) While the mean RH at z = 2 km reaches 85% in just about 18 hours, the RH at z = 5 and 8 km do not approach the same values until t = 42 h. Referring to the sequence of azimuthally averaged wind fields in Fig. 3, we note that the larger vortex did not begin to elevate and intensify until after this time. As we shall see below, this deep moistening of the core does not entirely precede the mid-level intensification in every case; in some cases they occur together, and in some the mid-level vortex begins to intensify before RH > 80% has been achieved throughout.

* The averaging is computed on model levels, which are defined by their hydrostatic pressure. Where we refer to altitude, we refer to the mean altitude of the model surface in the nested grid. These altitudes in fact change only a small amount (10 - 100 m) over space and time as the simulation evolves.

Fig. 4 Mean values of inner-core relative humidity (RH) averaged over a 160 km x 160 km box around the vortex centre for the surface vortex simulation, on model levels with approximate mean altitudes of z = 2, 5 and 8 km.

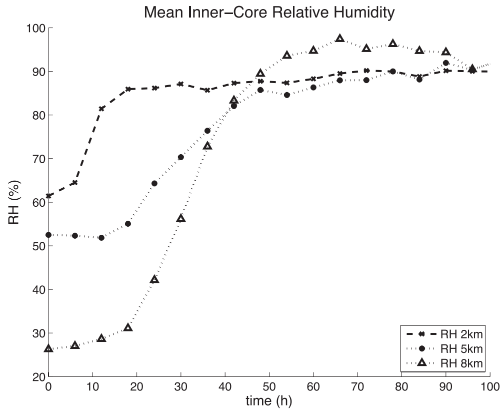

A more comprehensive view of the dynamic and thermodynamic evolution preceding TC genesis is presented in terms of time-height diagrams of the mean inner core values (using the same averaging 'box' as above) of RH, vertical vorticity, moist diabatic heating, potential temperature perturbation, vertical velocity, and horizontal divergence, as shown in Fig. 5 using hourly model output for the period t = 36 to 72 h. The RH diagram shows that the upper levels become moistened to near saturation (RH > 90%) by t = 45 hours, with distinct maxima of RH in the upper boundary layer, at the freezing level, and around z = 9 km. As the upper-level RH increases, so does the upper-level diabatic heating, though it is defined more by increasingly large 'bursts' rather than by a steady rise.

After 55 hours, larger heating rates begin to appear in the middle and lower levels (as seen by the lowering of the higher-value contours), at which time the mid-level vorticity begins to increase more rapidly. While the potential temperature perturbation (defined as the difference between the inner core value and the mean over the inner grid) is steadily increasing aloft, it actually decreases at low and middle levels. While this is of course required by thermal wind balance, it is also consistent with the proposition that some mesoscale vortices become 'cold-cored' before TC genesis (Bister and Emanuel 1997; Emanuel 2005).

As discussed in the introduction, the relative roles of stratiform and deep convection in the genesis process remain an open question. Mapes and Houze (1995) used vertical profiles of area-averaged horizontal diver-

Fig. 5 Time-height diagrams of mean values of inner-core variables averaged over a 160 km x 160 km box centred at the vortex centre using hourly model output from t = 36 to 72 hours in the surface vortex case: (a) RH; (b) vorticity; (c) moist heating; (d) potential temperature perturbation (relative to the mean over the inner grid); (e) vertical velocity; (f) divergence. Dashed contours indicate negative values, and zero contour is thickened.

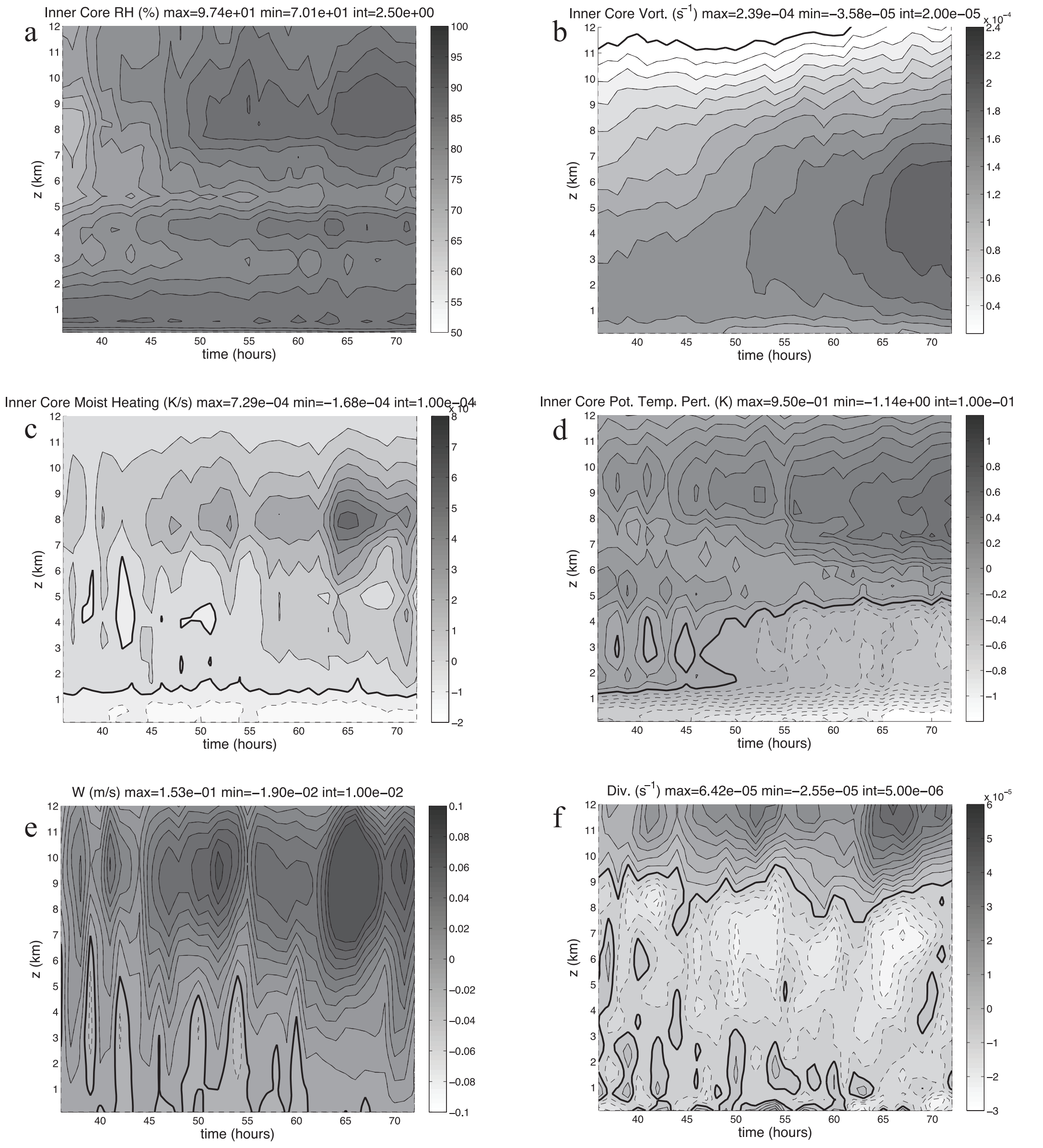

gence to identify the relative amplitudes of stratiform and deep convection in Tropical Pacific mesoscale convective systems. Time-height diagrams of vertical velocity and divergence are shown in the bottom panels of Fig. 5. Before t = 60 h, each pulse of deep convection (as also indicated by the moist heating) is followed by a brief period of mean downdraughts at lower altitudes, with corresponding peaks in positive low-level divergence. The persistent maximum in convergence from z = 6 to 8 km indicates a divergence profile that is consistent with stratiform precipitation, with embedded short periods of more convective profiles. However, as can be seen by the updraught plumes in Fig. 2, and as will be shown in the next section, both deep convective towers and stratiform precipitation are present throughout the simulation.

The vertical structure of the divergence profiles can be seen more clearly in Fig. 6. To generate these curves, the time-height data have been smoothed with a 1-2-1 filter, twice in the temporal direction, and once in the vertical. A mix of stratiform and deep convective activity is evident at all three times leading up to genesis (t = 40, 50 and 60 h), but a large increase in low-level convergence (t = 65 h) does not occur until just about the same time as the formation of the low-level vortex (between t = 60 and 66 h).

CFAD analysis of changes in convection

We may further analyse the changes in the dynamic and thermodynamic properties of the convection by looking at distributions of the frequency of occurrence for values of various model variables as a function of height. This method was first used by Yuter and Houze (1994) to analyse the evolution of vertical motion and reflectivity in a mid-latitude mesoscale convective system, inventing the term 'contoured frequency by altitude diagram', or CFAD. Rogers et. al. (2007) used CFAD analyses to compare the distributions of rainfall and reflectivity in simulated tropical cyclones to those observed by airborne Doppler radar.

The data used are the values of each variable at each height in a 200 km x 200 km box around the centre of the cyclone, divided into 30 equal bins between the values shown on the x-axis in each plot. To better view the large range of frequency values in these two-dimensional contour plots, we add 1.0 x 10^{-4} to the frequency values everywhere and then take the base 10 logarithm. Since the contour interval in all the diagrams is 0.4, a change of one contour corresponds to an increased frequency of $10^{0.4}$ = 2.51 of that value.

Figure 7 shows CFAD diagrams for vertical velocity, latent (moist) heating, and vertical vorticity at t = 24 h and t = 60 h in the surface vortex simulation. The vertical velocity and latent heating diagrams have very similar structures. Both are highly peaked at the zero value and show distributions of warm updraughts and cool downdraughts on either side. The negative values of each are peaked at z = 4 km, while the positive values have two peaks, one near z = 2 km and the other near z = 9 km.

At a first glance, the figures on the left (24 h) and on the right (60 h) are not strikingly different. It seems that the frequency of downward motions and evaporative cooling is hardly changed between 24 and 60 h, even though the inner-core environment has achieved mean RH values of 80 to near 100 per cent (see Fig. 5(a)). Thus, the notion that downdraught activity ceases or even declines when the inner core becomes nearly saturated is not supported by this analysis. However, closer inspection of frequencies in the positive ranges shows that the frequency contours for w and LH have indeed shifted significantly to the right at 60 h, especially at higher altitudes. For example, at t = 24 h, the point w = 2 m s^{-1}, z = 10 km lies between the second and third contours. At t = 60 h, this same point lies between the fourth and fifth contours, implying a factor $10^{0.8}$ = 6.31 increase in the occurrence of 2 m s^{-1} updraughts at that altitude. Inspection of the latent heating diagrams shows a similar change. The vorticity diagrams show a seemingly equal spreading of the vorticity distribution in the positive and negative directions. While it is hardly evident to the eye, there is in fact a significant increase in the mean vorticity at higher altitudes, as previously shown in the time-height diagram of Fig. 5(b).

Thus, a CFAD analysis of the relevant model output shows that as the vortex evolves toward the time of genesis, the frequency of occurrence of stronger and deeper convective updraughts steadily increases. Surprisingly, the frequency of cool downdraughts does not appear to diminish much, or at all, in the hours before TC genesis.

Fig. 6 **Smoothed profiles of the mean inner-core divergence data for the surface vortex case.**

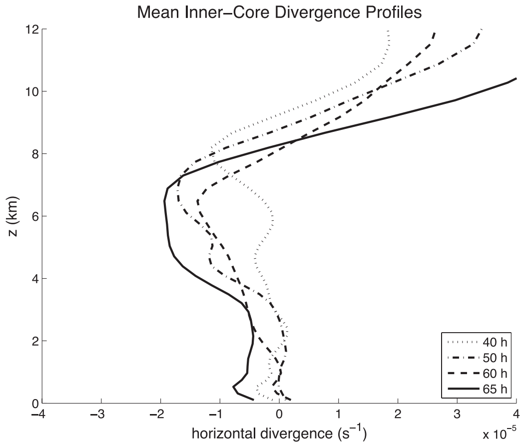

Genesis sensitivity to initial vortex structure and sounding

A mid-level vortex case

While the surface vortex initial condition used is highly unrealistic, we have used it in the first analysis because the evolution of the wind field emphasises the changes in the inner core preceding TC genesis,

Fig. 7 Contoured frequency by altitude diagrams (CFADs) for vertical velocity (upper panels), latent (moist) heating (middle panels), and vorticity (lower panels) at *t* = 24 h (left side) and *t* = 60 h (right side) in the surface vortex simulation. The mean value at each altitude is indicated by the thick line near the centre.

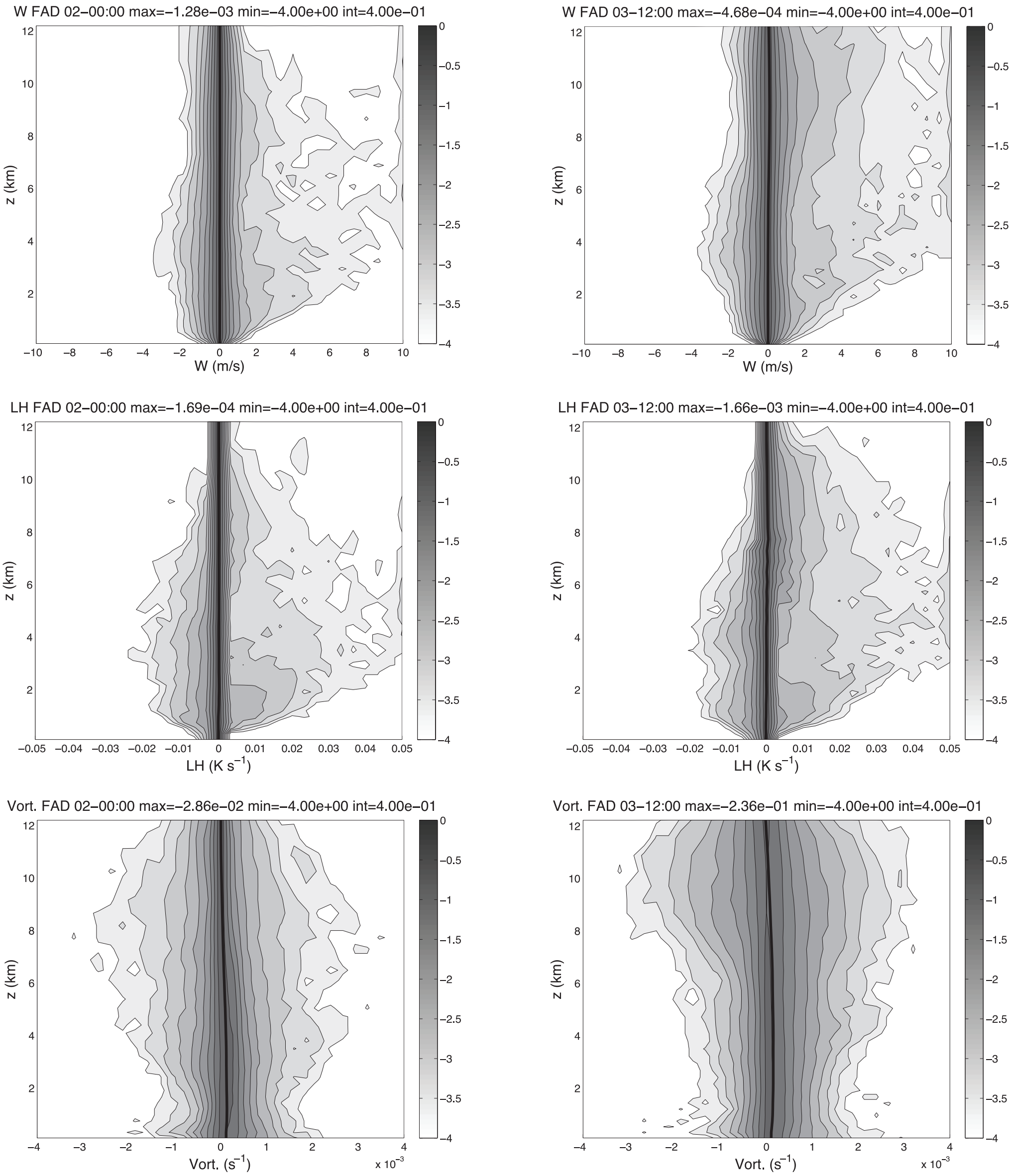

especially the appearance and intensification of a mid-level vortex which was not initially present. Nonetheless, it is natural to wonder if the evolution would be different for a more realistic initial vortex, particularly one with a pre-existing mid-level vortex and a much weaker surface circulation. Since the development of a mid-level vortex was a precursor to genesis, does the pre-existence of a mid-level vortex promote a more rapid development?

With this in mind, we consider a 'mid-level vortex' simulation. The initial vortex has the same azimuthal wind profile as the surface vortex case, but with z_{max} = 3720 m, such that the circulation is a weakly baroclinic, mid-level vortex which is representative of the precursor disturbances that most often lead to TC genesis in the real atmosphere, such as monsoon depressions, mesoscale convective vortices (MCVs), and easterly waves, all of which are 'cold-core' cyclones in the lower troposphere. The vertical structure parameters L_z and α are chosen such that the maximum surface wind speed is exactly half (5.0 m s^{-1}) of the wind speed at z_{max}. Numerical values for the parameters for this vortex and for the others to follow are listed in Table 1.

The initial wind field for this vortex is shown in Fig. 8(a). Plots of six-hourly pressure anomaly and surface wind are very similar to those of the surface vortex case, but indicate a slightly later genesis time and a slower acceleration of intensification (Fig. 8(b)). However, the hourly model output from t = 36 to 84 hours (Fig. 8(c)) shows some significant differences from the surface vortex case. Rather than remaining constant, the surface pressure anomaly is very slowly strengthening in the 24 hours before genesis. An evident 'jump' in the pressure anomaly which we might associate with genesis of a smaller-

Table 1. Vertical structure parameters and soundings for the initial vortices used in this study. Asterisks (*) indicate values that are the same as for the surface vortex simulation.

Name	L_z *(m)*	α	z_{max} *(m)*	*Sounding*
Surface vortex	5000	2.0	0	Jordan
Mid-level vortex	3175	*	3720	*
Deep vortex	6500	3.0	*	*
Shallow vortex	3000	3.0	*	*
Pre-saturated	*	*	*	RH 90% up to 12 km
Dry above 7 km	*	*	*	RH 5% from 7-12 km
Dry above 4 km	*	*	*	RH 5% from 4-12 km
Mid-level vortex, 1m/s surface wind	2015	*	4400	*
Mid-level vortex, 1m/s surface wind, pre-saturated	2015	*	4400	RH 90% up to 12 km

Fig. 8 Results for the mid-level vortex case: (a) initial zonal wind field; (b) maximum 10 m wind and negative surface pressure anomaly; (c) wind and pressure anomaly for one-hour model output from 36 to 84 h; (d) azimuthally averaged azimuthal wind field at t = 72 h.

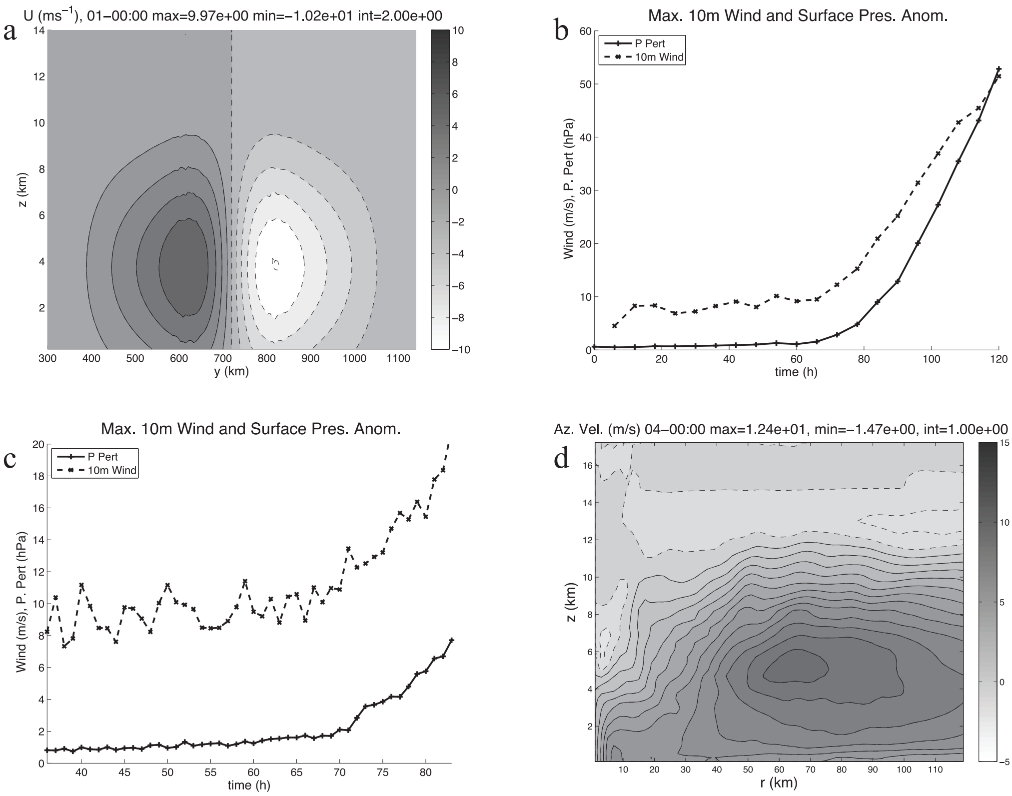

scale vortex does not occur until $t = 71$ hours. Figure 8(d) shows the azimuthally averaged wind field at $t = 72$ hours, when the small-scale surface vortex has just appeared, much as it did at $t = 63$ h for the surface vortex case. The wind field is remarkably similar to that shown for the surface vortex case (Fig. 3(d)), with a radius of about 60 km for the mid-level vortex, and a maximum mid-level wind speed of 12 m s^{-1}. Both vortices evolved to the same dynamic structure before genesis.

Time-height diagrams of the inner core fields for this case as shown in Fig. 9 are similar to those of the surface vortex case (Fig. 5), but with some interesting differences. The upper-level humidity is lower at $t = 42$ h in this case than it was at $t = 36$ h for the surface vortex. This is due to the higher temperatures of the more intense warm core necessary to balance the elevated and more baroclinic vortex. The near-saturation of the inner core column is delayed by about 12 hours. Again, intensification and additional elevation of the mid-level

Fig. 9 Time-height diagrams of mean values of inner-core variables averaged over a 160 km x 160 km box centred at the vortex centre using hourly model output from $t = 42$ to 78 hours in the mid-level vortex case: (a) RH; (b) vorticity; (c) moist diabatic heating; (d) potential temperature perturbation (relative to the mean over the nested grid); (e) vertical motion; (f) horizontal divergence.

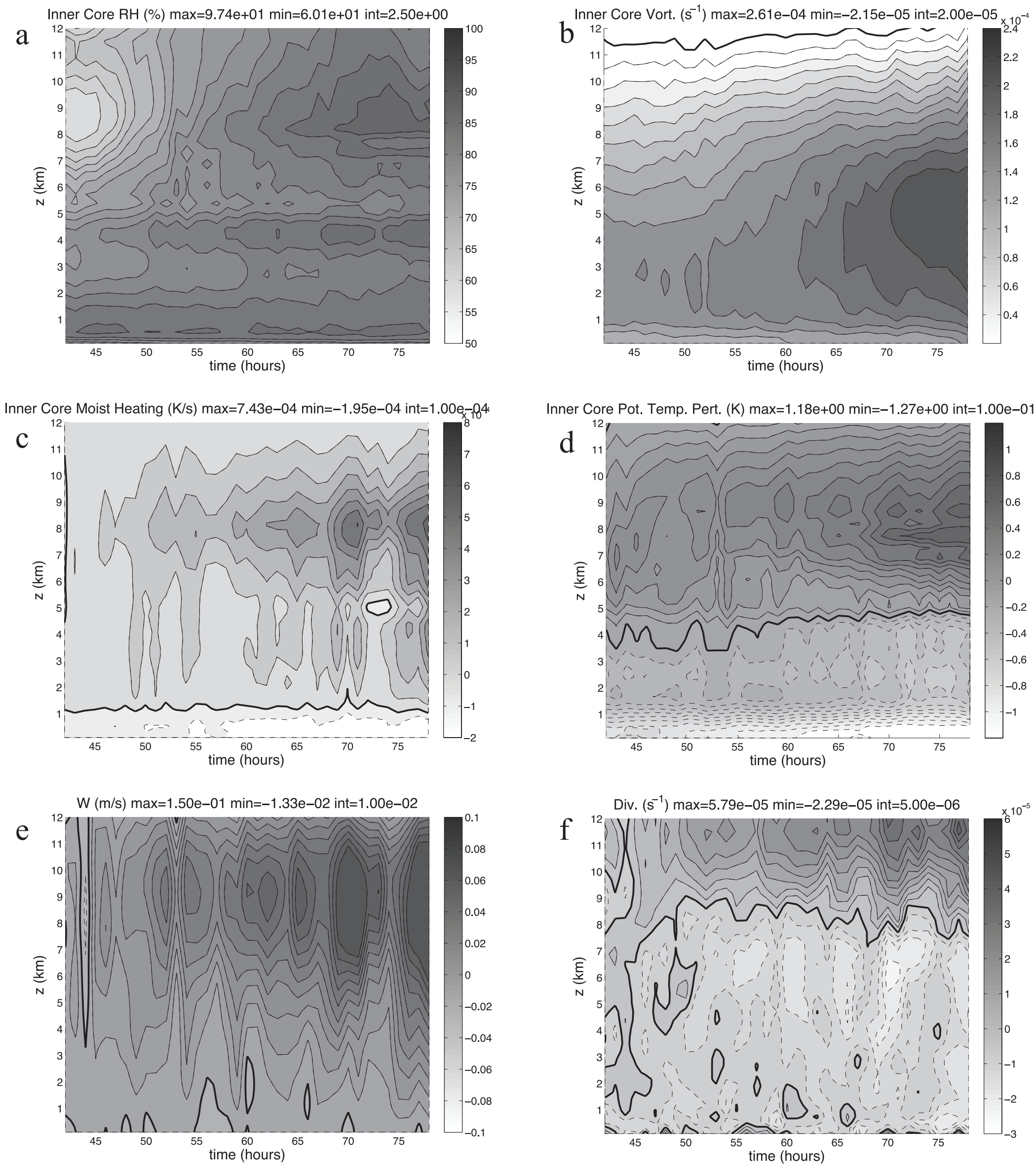

vortex begins around the same time as this near-saturation is achieved. Larger values of positive diabatic heating begin to appear at lower levels just before this time as well. The vertical motion and divergence profiles evolve in a similar manner to the surface vortex case, with stratiform-type convergence evident early on, but persistent convergence developing at lower and lower levels as the time of genesis is approached.

CFAD diagrams for the mid-level vortex case, accounting for the eight-hour delay in the time of genesis, were extremely similar to those of the surface vortex case, and thus are not shown.

Deeper and shallower surface vortex cases

To further evaluate how the vortex wind field evolves in the time before TC genesis, we performed additional simulations based on the surface vortex case, but with the initial wind field made deeper and shallower. Changes to the parameters L_z and α in Eqn 4 that define the deep and shallow vortices are listed in Table 1.

The initial condition, intensity evolution, and time-height diagrams of inner-core RH and vorticity for the deep vortex case are shown in Fig. 10. TC genesis and rapid intensification occur about 12 hours earlier than for the original surface vortex case. Near-saturation of the upper levels occurs about six hours earlier than in the original vortex case (compare Fig. 10(c) to Fig. 4 or Fig. 5(a), and note different time ranges on the x axis). The mid-level vortex begins to elevate and intensify when the middle and upper-level humidities are about 70 per cent, a lower value than for the previous cases, but certainly substantial moistening has occurred before mid-level intensification begins. The increased rate of development is most likely due to dynamical reasons, since the surface circulation decays less and the mid-level vortex develops more quickly due to the increased mid-level vorticity.

Results for the shallow vortex case, shown in Fig. 11, are a little more interesting. Noting the longer time range on the x-axes of the figures, we see that the evolution is similar to those shown above, but the time to genesis is about 36 hours longer, and the low-level circulation is clearly weakening up until that time. Near-saturation of the middle and upper levels of the atmosphere, however, comes at around 48

Fig. 10 Results for the deep vortex case: (a) initial zonal wind field; (b) maximum 10 m wind and negative pressure anomaly; (c) time-height diagram for mean inner-core RH from six-hourly model output from 0 to 72 h; (d) time-height diagram for mean inner-core vorticity.

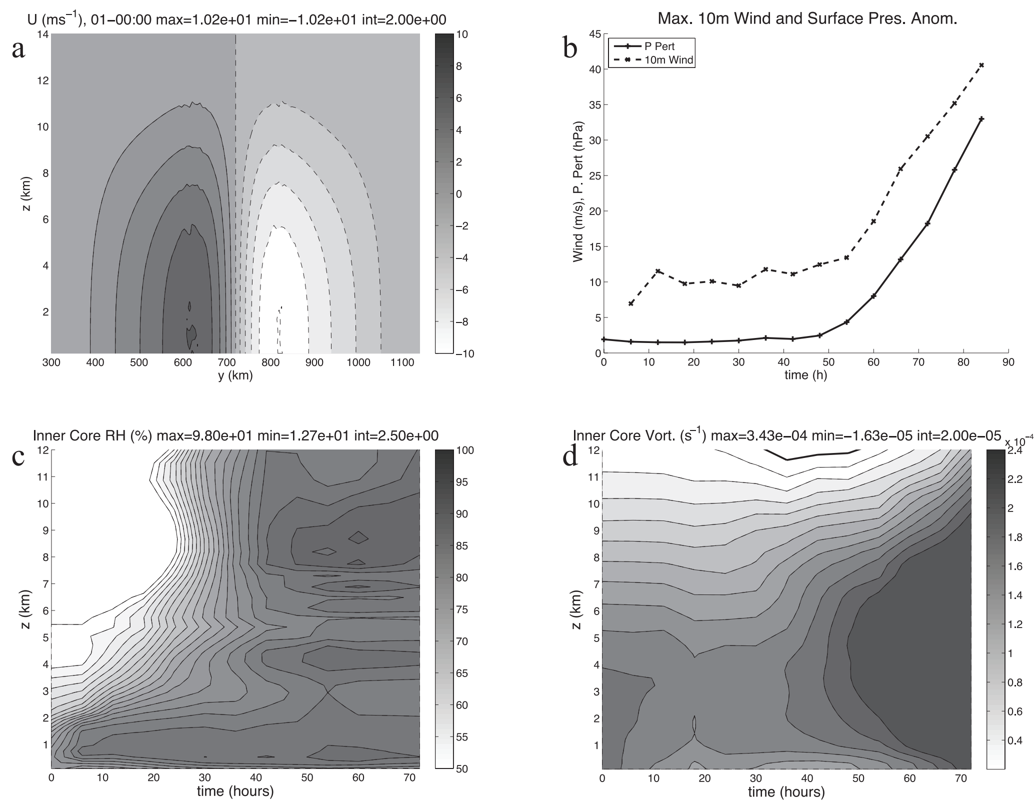

Fig. 11 **Results for the shallow vortex case: (a) initial zonal wind field; (b) maximum 10 m wind and negative pressure anomaly; (c) time-height diagram for mean inner-core RH; (d) time-height diagram for mean inner-core vorticity; note different time axes, from 0 to 120 h, and the later genesis time.**

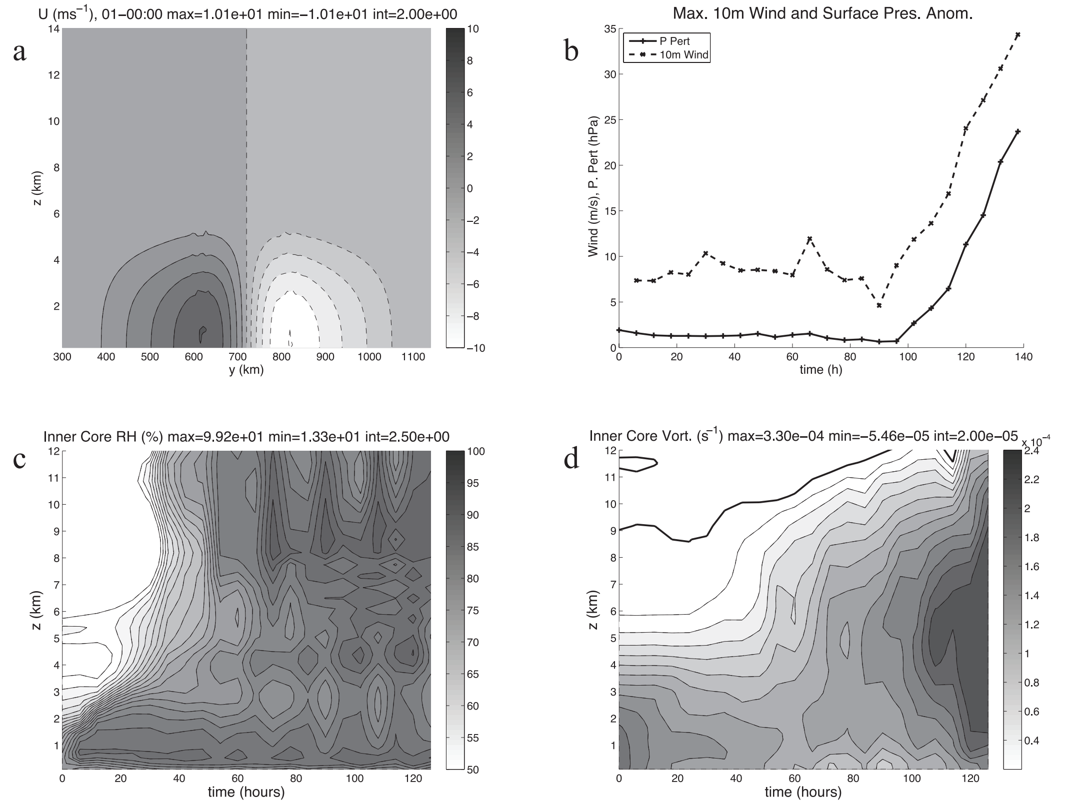

hours, only a little later than for the previous cases. Development of the mid-level vortex takes substantially longer, and this seems to be the primary cause of the delayed genesis. However, an additional factor may be the unsteadiness of the upper-level RH after the initial near-saturation around t = 48 hours. Looking carefully at the time-height diagram for RH, its values oscillate between values of 80 and 95 per cent during the period in which the mid-level vortex is developing. These pulses of increased RH and the convection which causes them (not shown) are reminiscent of the diurnal cycle of convection seen in mesoscale convective complexes leading up to tropical cyclogenesis as discussed by Zehr (1992). However, they are probably for different reasons, as further discussed below.

Changes in upper-level humidity

To explore the role of the mid and upper-level humidity in controlling the genesis process, we performed additional surface vortex simulations with the environmental sounding modified so as to have RH = 5% from z = 7 to 12 km and from z = 4 to 12 km, and a third simulation with the RH = 90% from the surface to 12 km. The results of these simulations are presented in Fig. 12. As shown in the top two figures, setting the RH to five per cent above 7 km only delays genesis by about six hours. The amount of water necessary to saturate the atmosphere at altitudes above 7 km is very small, so we surmise that the first few deep convective bursts can achieve near-saturation almost as quickly as when the initial RH is 30 to 50 per cent between 7 and 12 km (as it is for the Jordan sounding). Setting the RH to five per cent above 4 km, however, has a profound effect, delaying upper-level near-saturation until t = 66 h and genesis until t = 96 h (note different time axes in each figure). As shown above, the development and intensification of the mid-level vortex does not occur until after upper-level near-saturation has been achieved.

As one might expect, genesis occurs extremely quickly for the surface vortex with RH = 90%.

Fig. 12 Time-height diagrams of the mean inner core RH (left side) and vorticity (right side) for the simulations that are initially dry (5% RH) above 7 km (top panels), dry above 4 km (middle panels), and pre-saturated (90% RH) from 0 to 12 km (lower panels); note different time axes in each case.

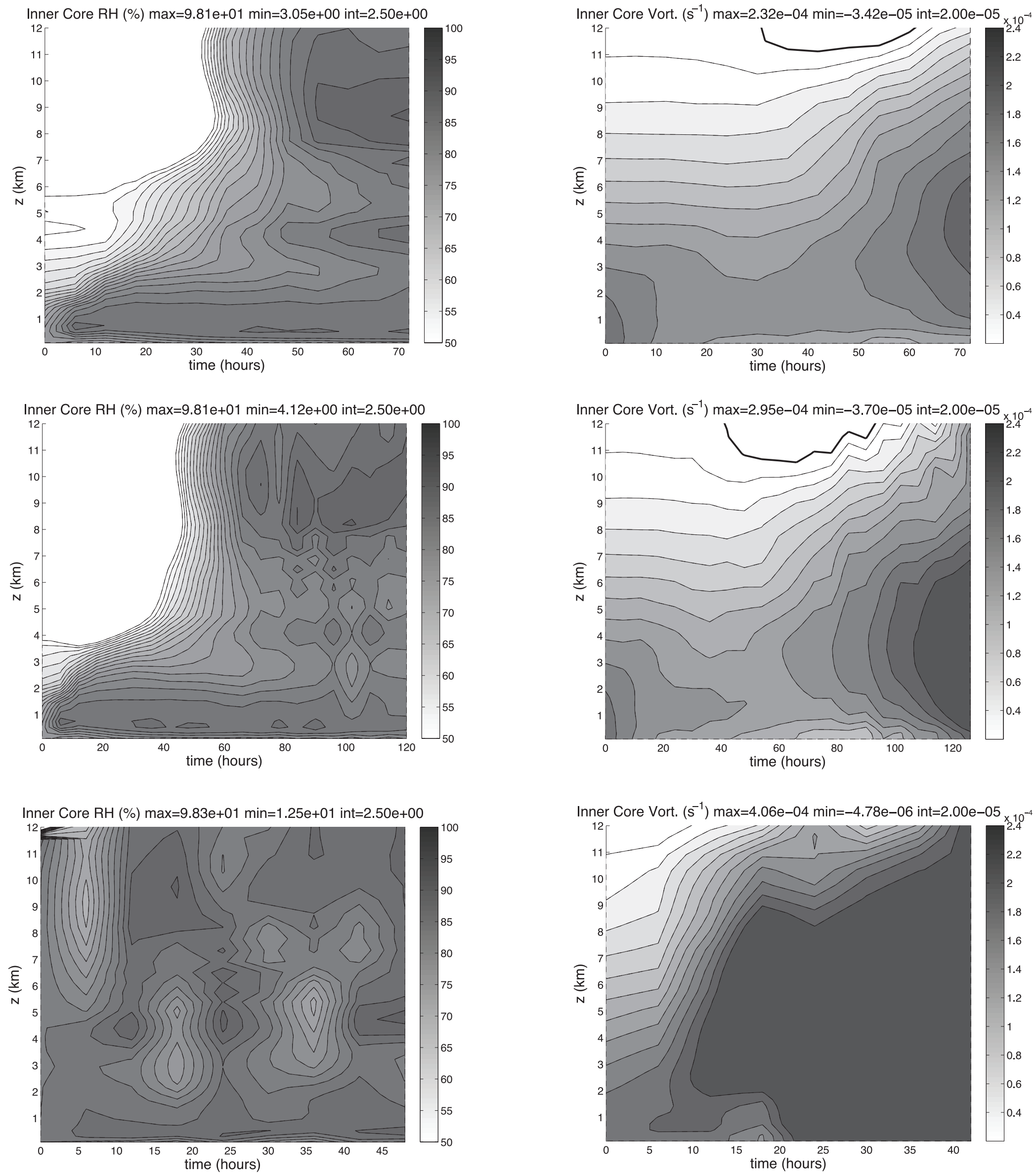

Nonetheless, the wind field is found to go through a similar evolution with the development of a mid-level vortex (although the surface vortex has hardly any time to decay) and then the appearance of a smaller-scale surface vortex which evolves into the tropical cyclone. The mid-level vortex is generated in just the first 12 hours by an initial round of widespread convection in the inner core that rises all the way to the tropopause (not shown). A second burst of convection at t = 20 h generates the smaller-scale surface vortex, which by t = 36 h has a clearing eye, a coherent eyewall, and distinct boundary-layer inflow and upper-level outflow layers that are common to intense cyclones.

Fig. 13 Results for the mid-level vortex with 1 m s^{-1} surface winds and a pre-saturated environment: (a) initial zonal wind field; (b) maximum 10 m wind and negative pressure anomaly; (c) time-height diagram for mean inner-core RH; (d) time-height diagram for mean inner-core vorticity; note different time axes.

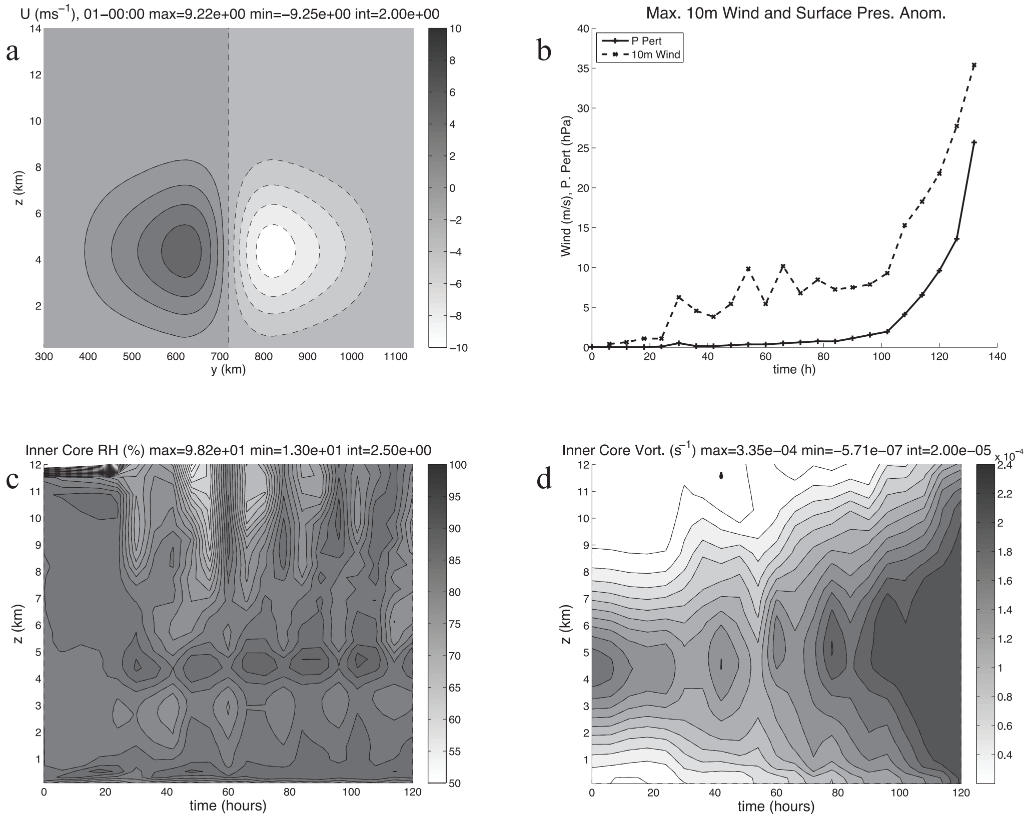

Mid-level vortex with very weak surface winds

Finally, we performed two additional simulations that began with a mid-level vortex with v_{max} = 10 m s^{-1}, but with the vertical structure changed so that the initial surface wind speed was only 1 m s^{-1}. One simulation had the Jordan sounding while the other had RH = 90%. With the Jordan sounding, almost no progress had been made toward TC genesis after six full days of model simulation (results not shown). With RH = 90%, TC genesis occurred around t = 100 h as illustrated in Fig. 13. Interestingly, upper-level RH declines after the first convective burst, and takes another 60 h to become persistently moistened again. During this time, the simulation exhibits similar repeated cycles of pulsing convection leading up to genesis as was seen before in the shallow vortex case (Fig. 11(c)), and in the RH = 90% surface vortex case (Fig. 12, lower left panel).

This convective pulsing is more clearly illustrated in Fig. 14, which shows time-height diagrams of vertical velocity and total condensate (cloud ice, snow, graupel, cloud water, and rain) for one-hourly data from t = 36 to 72 h. Each enhanced convection period is followed by a period of mean downdraughts, with the next convective period beginning almost immediately after the last has reached 12 km height. The decline in the condensate that immediately follows the updraught indicates significant precipitation and evaporation, which is likely responsible for the diabatic cooling (not shown), downdraughts and subsequent upper-level drying (Fig. 13(c)) at these times. The two bottom panels of Fig. 14 show horizontal sections of the diabatic heating at z = 6.5 km, t = 54 h, in the middle of the strong updraught period, and at t = 61 h, in the middle of the downdraught period that immediately follows. These plots show that these updraught cycles are not representative of just one or a few large updraughts (as one might imagine in an environment that starts with RH = 90%), but rather they indicate enhanced widespread small-scale updraught activity, followed by suppressed activity with enhanced downdraught regions.

Fig. 14 **Variations in convective acitivity associated with the pulsing of convection as seen in the mid-level vortex with 1 m s^{-1} surface wind and RH = 90%, depicted in Fig. 13: (a) time-height diagram of mean inner core vertical velocity; (b) time-height of total condensate; (c) diabatic heating and wind vectors at *t* = 54 h, *z* = 6.5 km; (d) diabatic heating and wind vectors at *t* = 61 h, *z* = 6.5 km.**

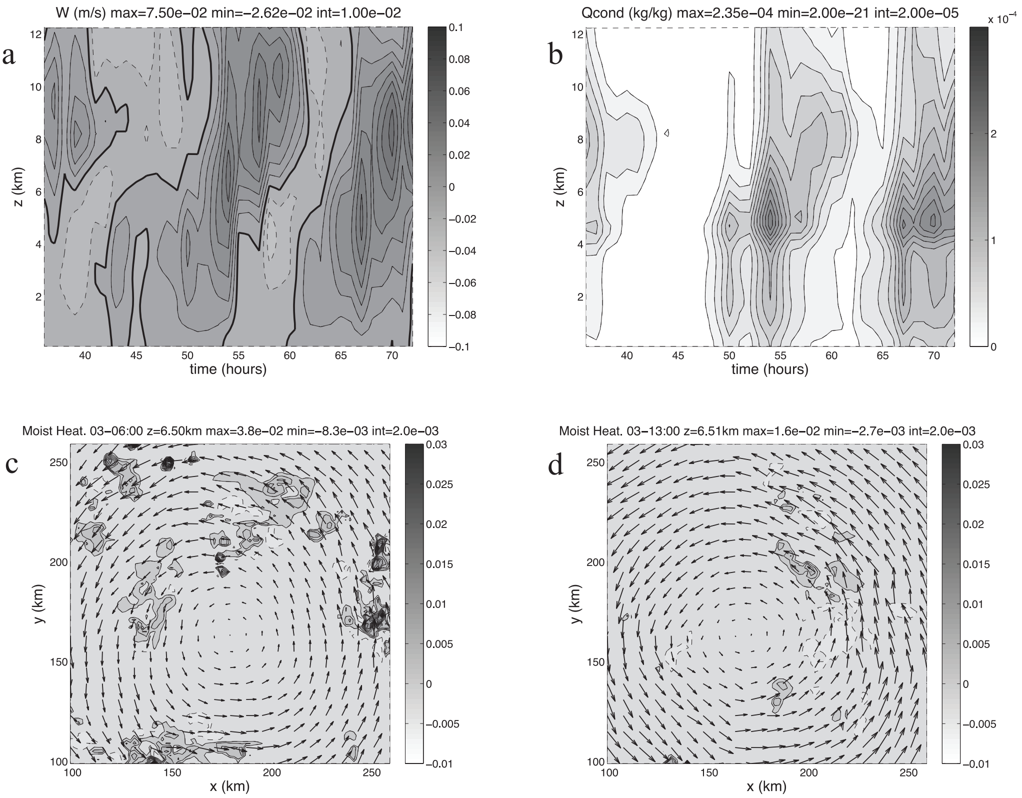

Further investigation of this pulsing phenomenon revealed it to be an artifact caused by the interaction between three unrealistic aspects of these particular idealised simulations: the nearly pre-saturated (RH = 90%) initial state, the doubly periodic boundary conditions, and the relatively small size of the outer domain. Due to the near-saturation, the initial 'burst' in convective activity has numerous deep updraughts. This large convective burst leads to a fairly coherent gravity wave radiating outward from the centre of the domain with a phase speed of about 25 m s^{-1}. The leading edge of this wave returns to the centre of the domain in about 16 h, leading to an excitation of new convective activity. When this simulation was repeated with a third outer nest with 160x160 grid-points and 18 km grid spacing (thus doubling the size of the outer domain), the convective pulsing disappeared.

The surface vortex simulation was also repeated with the additional outer grid. The result was nearly identical to the simulation with two grids, with genesis (as defined by formation of the new surface vortex) at *t* = 62 h.

Further analysis

Vortex merger and axisymmetrisation

As discussed in the introduction, a series of recent papers has proposed that the formation, mutual interactions, and mergers of small-scale vortices generated by vorticity tilting and stretching in strong convective updraughts (VHTs) play a significant role in the TC genesis process. Here, we only briefly describe the extent to which vortex merger does occur in these simulations, as a detailed documentation would require numerous additional figures, and it is not our goal to either challenge or critique the VHT hypothesis.

A review of the vertical vorticity fields and moist heating fields of all the simulations (a few of which will be shown below) shows that there is, of course, considerable generation of small-scale vorticity anomalies by convective updraughts. The vorticity anomalies were mostly positive at low levels (where they are mostly generated by low-level convergence of the surrounding positive vorticity), but had a wide distribution of both signs at middle and upper levels, where there is significant upward advection and stretching of tilted horizontal vorticity. These differences are evident in the vorticity CFAD diagrams of Fig. 7. Nonetheless, vortex 'merger' was not the dominant mode of interaction and intensification. After generation by convection, most of the vorticity anomalies are sheared and axisymmetrised by the larger circulation, rather than coalescing with the other nearby, stronger vortices. Very few of the vorticity anomalies were even close to being 'closed circulations' in the absolute sense, thus making the concept of axisymmetrisation more applicable than vortex merger.

In almost every case where a distinct vortex merger occurred, the merger was strongly diabatically forced, one or both of the low-level vortices was coupled to an updraught, and the low-level convergence forced by the updraught brought two or more vortices together, leading to a single, more intense vorticity anomaly; this is essentially the diabatic vortex merger process proposed by Hendricks et al. (2004). At the same time, many of the 'events' of low-level intensification occurred in isolation, driven by the convergence and stretching of a strong convective updraught in the immediate vicinity. Vortex merger was also more frequent where the surrounding cyclonic flow was weaker, such as at middle levels in the shallow vortex case, or low levels in the 1 m s^{-1} surface wind case.

If there are any significant differences between our results and those of Montgomery et al. (2006), they may be explained by this last observation. Their control simulation was initialised with a smaller and weaker mid-level vortex ($v_{\max}$ = 6.6 m s^{-1}, RMW = 60 km), allowing for stronger interactions between the convectively generated vorticity anomalies embedded in the weaker mesoscale circulation.

The run-up to genesis

To those familiar with vortex dynamics or tropical cyclone development, it would seem obvious to the eye that the changes in the vortex structure in the 24 hours before genesis, shown in previous figures (e.g. Fig. 3, Fig. 5(b), etc.), would make the vortex more and more likely to develop into a tropical cyclone. But how can we quantify these changes?

One way to evaluate the propensity of a vortex for tropical cyclone development is to measure the efficiency with which latent heat released in convection can be converted into the kinetic energy of the cyclonic wind field, thereby leading to further development. Schubert and Hack (1982) and Hack and Schubert (1986), using an updated version of the Eliassen (1951) balanced vortex model, computed efficiencies of exactly this type using both analytical and numerical methods for vortices of various shapes and sizes. Not surprisingly, they found that as the vortex intensifies, the efficiency increases substantially. However, the use of a balanced model which assumes a balanced response to slowly varying, axisymmetric heat sources left some uncertainty as to the precision of their results.

Building on these ideas, and using the linear, but nonhydrostatic and time-dependent models of Nolan and Montgomery (2002) and Nolan and Grasso (2003), Nolan et al. (2007) were able to show that the vortex intensification by latent heat release does not depend on its distribution in time, but only on the net azimuthally averaged heating. Using their nonhydrostatic model, they too computed the 'kinetic energy efficiency' for vortices of varying intensities. Interestingly, they found that mid-level vortices were slightly more efficient than surface vortices of the same strength.

Figure 15 shows the kinetic energy efficiency (KEE) of the azimuthally averaged vortex wind field for the surface vortex case at t = 36 and t = 60 h. These figures show the fraction of azimuthally averaged heat energy released at each point in the (r, z) plane that is converted to kinetic energy of the symmetric wind field during the adjustment process. Not surprisingly, the largest efficiency is found at the centre of each vortex, with the maximum values from z = 8 to 10 km, since heating at this altitude can drive convergence over the depth of the vortex. The negative values at lower altitudes are indicative of the fact that low-level heating will drive divergence at the level of the mid-level vortex. Although it would also intensify the low-level wind field, it weakens the vortex where it is strongest, thus decreasing kinetic energy. Comparing the results for the two times, the maximum efficiency for the vortex increases by a factor of four from t = 36 to 60 h.

The peak value of KEE is not a very representative measure of the efficiency, since it exists only at a single point (r = 0) and at high altitude. To reduce the spatially varying KEE fields to a single representative number, Nolan et al. (2007) defined the 'relevant' KEE as the volume-averaged KEE over some region where the most convective heating is likely to occur. For vortices that have already developed a strong low-level circulation, the relevant area is around the RMW. However, the most active area of convection for genesis seems to be inside the RMW, and most of the latent heat release is above 4 km and below 10 km (see e.g., Fig 5(c)). For this purpose, we define the relevant KEE to be the volume averaged KEE in the region $0 \le r \le 40$ km, 4 km $\le z \le 10$ km. Figure 15(c) shows the relevant KEE as a function of time from hourly model output leading up to the time of genesis for the surface vortex and mid-level vortex cases. In each case, the relevant KEE begins a steady and accelerating rise about 24 hours *before* genesis, more than doubling in each case.

Fig. 15 Kinetic energy efficiency analyses of the vortex wind fields: (a) KEE for the surface vortex case at t = 36 h; (b) KEE at t = 60 h; (c) relevant KEE in the 24 hours before genesis for the surface (o) and mid-level (×) vortex cases; (d) relevant genesis KEE for the same cases.

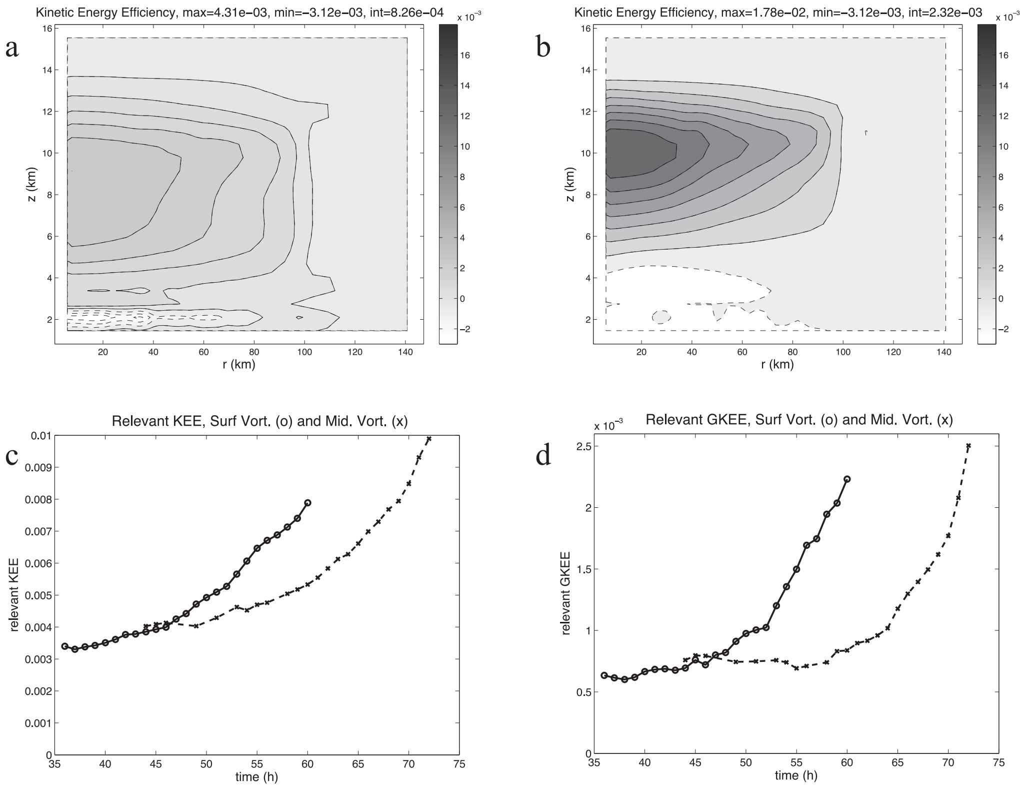

The development of a smaller-scale, low-level vortex has been seen to be the defining moment of genesis in our simulations. To try to capture the efficiency of the larger vortex in low-level intensification, the KEE calculation was modified to compute the fraction of heat energy which leads to an increase in the kinetic energy of the wind field only in the region $0 \le r \le 40$ km, $0 \le z \le 6$ km. We call this efficiency the ‘genesis’ KEE (GKEE). To compute the relevant GKEE, we use the same averaging region defined above. As shown in Fig. 15(d), the relevant GKEE is much smaller than the KEE, but its value increases by more than a factor of three and over a shorter time period in the hours before genesis.

The moment of genesis

One of the striking aspects of the simulations presented above is the very short time over which the smaller-scale, low-level vortex forms at the surface. The rapid increase of the low-level vertical vorticity is nicely illustrated by CFAD diagrams computed on hourly model output from the mid-level vortex case, as shown in Fig. 16, for t = 70, 72 and 74 h (results were similar for the surface vortex case). While the distribution of frequencies of vorticity values is nearly unchanged at most altitudes, we can see at low levels the rapid appearance of much higher vorticity values. As shown in Fig. 7 for the surface vortex case, no such expansion of the range of positive vorticity values was seen in the time period from 39 hours before to three hours before genesis (and the results from the mid-level vortex simulation were nearly identical at those times).

How is this intense low-level vertical vorticity generated? Continuing with the mid-level vortex case, Fig. 17 shows the azimuthally averaged vertical vorticity and moist heating at t = 70, 71 and 72 h. At t = 70 h (upper panels), the highest values of vertical vorticity are confined in a very shallow layer at the vortex centre (where the centre is defined by the smoothed surface pressure minimum). At the same time, there is a broad distribution of moist heating in and around the core of the vortex, with a (radially) local maximum at r = 15 km. However, the

Fig. 16 CFAD diagrams of vertical vorticity at (a) t = 70 h, (b) t = 72 h, and (c) t = 74 h in the mid-level vortex case.

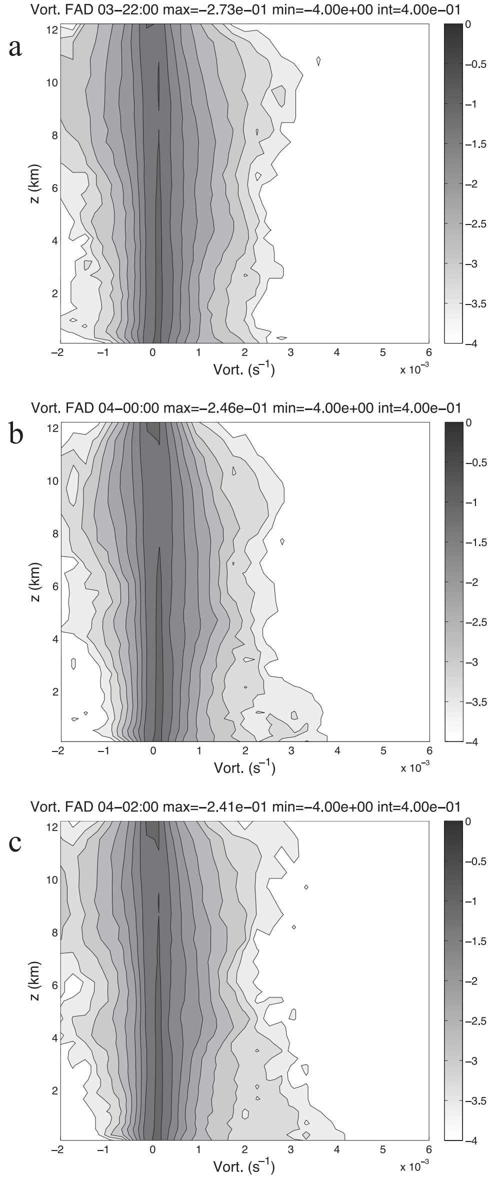

azimuthal averaging gives a misleading picture. The convection and moist heating at this stage are not organised and are still confined to isolated intense updraughts, with the peaks in the azimuthally averaged field corresponding to the radial positions of these updraughts. At 71 h, however, convection (and latent heat release) begins to occur closer to the vortex centre, and at 72 h the maximum heat release is occurring directly over the centre, with substantial additional heating within 10 km of the centre. The azimuthally averaged vorticity shows an enormous intensification and deepening of the central vorticity maximum in this one-hour period.

The large increase in moist heating near the vortex centre is associated with a single, long-lived updraught, with additional contributions from nearby updraughts. However, none of these updraughts is notably stronger than those in the surrounding area. This is illustrated in Fig. 18, which shows horizontal sections of low-level vorticity at $z = 0.5$ km and mid-level diabatic heating at $z = 5.0$ km at the same times. In these figures, each plot is centred at the location of the smoothed pressure centre used to compute azimuthal averages. At $t = 70$ h, near the surface, the wind field is characterised by an area of vorticity > $5.0\text{x}10^{-4}$ s^{-1} of 20-40 km in scale, embedded with, and surrounded by, smaller blobs of more intense vorticity with values up to $2.5\text{x}10^{-3}$ s^{-1}. A cluster of diabatic heating is located at $x = 170$ km, $y = 185$ km. It is interesting to note that the wind vectors are quite divergent around this cluster, suggesting this is the top of a new updraught.

One hour later, the pressure centre of the vortex has moved slightly to the west, perhaps in response to this central updraught. A new, connected series of clusters of deep convection has developed a little further to the west as well. These contribute to the additional local maxima in the azimuthally averaged heating in the radial range of 20-40 km from the centre (Fig. 17, right middle panel).

While these new updraughts seem to have faded after an additional hour, the 'main' updraught continues and moves even closer to the vortex centre (or perhaps, the centre moves closer to it). In the azimuthally averaged fields, the greater part of the appearance of this convection as being more intense is due to the fact that the convection occurs closer to the centre of the azimuthal averaging procedure. This results in substantially larger values of the azimuthally averaged heating, even though the heating rates in the individual updraughts are not much greater. However, the proximity to the vortex centre of this heat release is dynamically very important, as has been shown in the efficiency analyses above.

A review of the other simulations revealed a very similar series of events in each case: the trigger for the development of the smaller-scale surface vortex was the appearance of a single strong updraught, or cluster of updraughts, very close to the vortex centre. This updraught was also long-lasting, resulting in the formation of a single low-level vorticity anomaly that was significantly stronger than all the others. This vortex becomes the central core of the developing cyclone.

Fig. 17 Azimuthally averaged vorticity (left side) and moist heating (right side) for the mid-level vortex case at *t* = 70 (top), 71 (middle), and 72 h (lower panels).

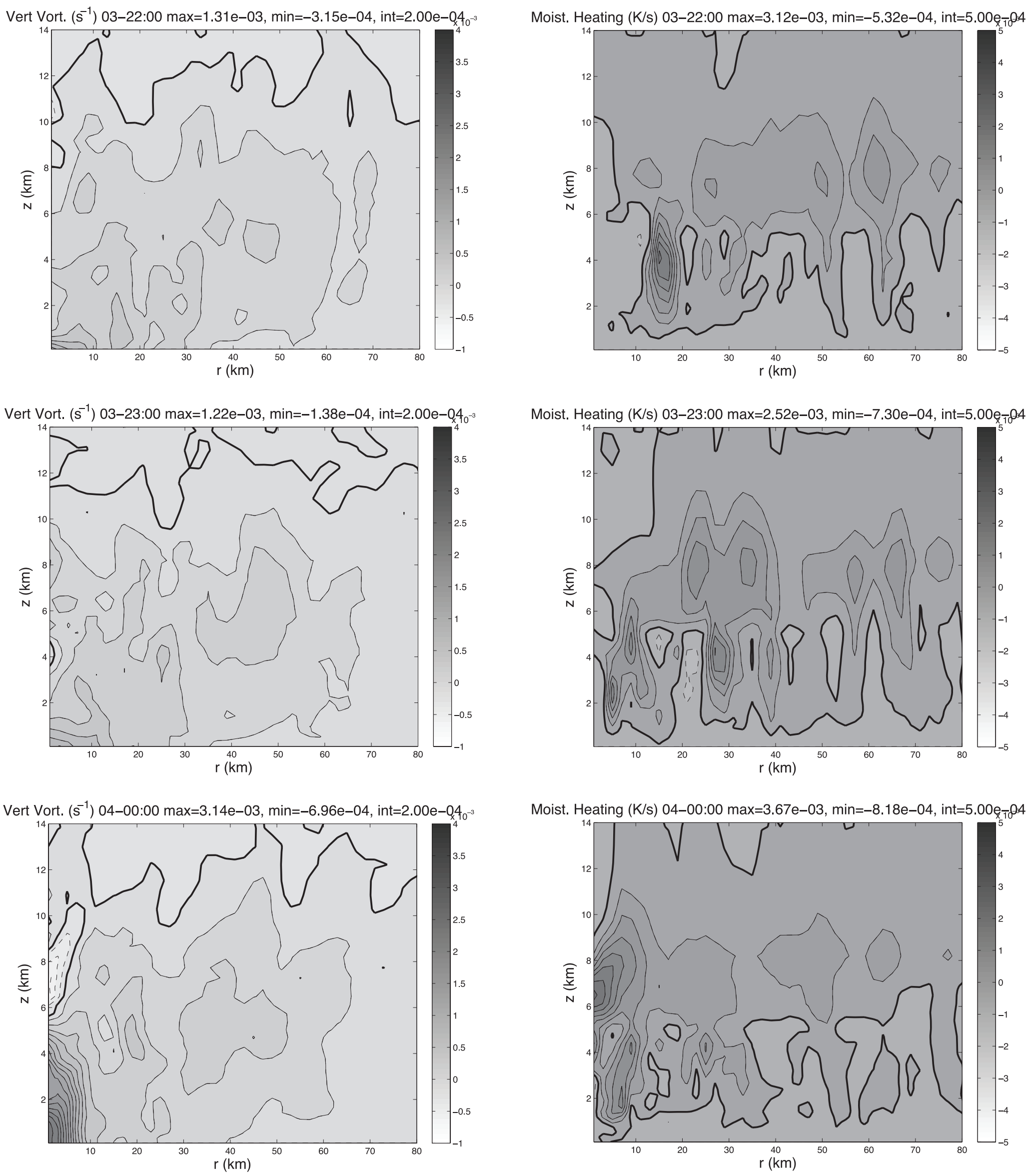

Conclusions

Summary

This study has presented simulations of tropical cyclogenesis in highly favourable, idealised conditions, using a high-resolution, convection-resolving numerical model. Except for a simulation with an unrealistically pre-humidified environment, it was found that all of the simulations had an 'incubation time' of one to three days before TC genesis and rapid intensification began. When it occurred, TC genesis was marked by the very rapid appearance of a small-scale, low-level vortex near the centre of the surrounding mesoscale vortex.

Fig. 18 **Vertical vorticity at z = 0.5 km (left side), and moist heating at z = 5.0 km (right side), at t = 70, 71, and 72 h in the mid-level vortex simulation.**

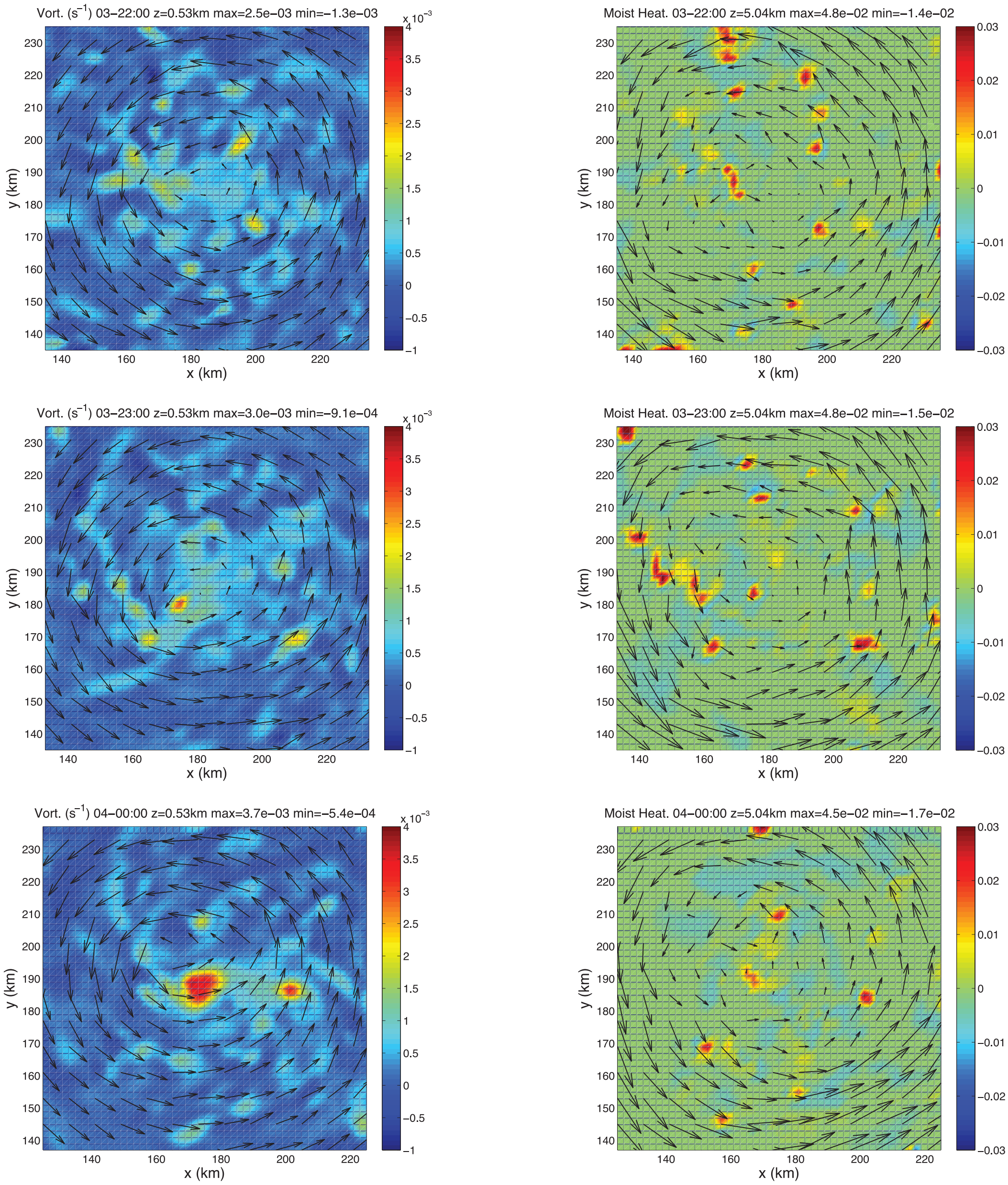

We attempted to identify critical changes in the moist dynamics and thermodynamics that occur in the vortex core in the days and hours before genesis. Bursts of deep convection in and around the vortex core began shortly after the beginning of each simulation, leading to a steady moistening of the atmosphere, with 'near saturation' developing quickly at low altitudes and then spreading upwards into the upper troposphere. As the relative humidity exceeded 80 per cent from the surface to 10 km, changes in the vortex wind field occurred that can be described as the formation (if not originally present) of a mid-level vortex that slowly contracted and intensified. If significant vorticity was already present in the middle and upper levels, mid-level vortex intensification began earlier, but still only after significant mid-level moistening had already taken place. In each case, when the mid-level vortex had contracted to a RMW of about 60 km, and a maximum wind speed of about 12 m s^{-1}, an even smaller vortex rapidly developed at the surface. This smaller-scale, low-level vortex would then grow into a rapidly developing tropical cyclone. The appearance of the small-scale, low-level vortex was marked by a sudden fall in the minimum surface pressure, with notable increases in maximum surface wind speeds not occurring until 6-12 hours later.

Changes in the character of the convection during the evolution toward genesis were evaluated with contoured frequency by altitude diagrams (CFADs). In the 24 hours before genesis, the frequency of stronger and higher penetrating updraughts increases, with corresponding increases in latent heat release. However, despite a substantial increase in middle and upper-level humidity during this period, the frequency and intensity of cool downdraughts showed little or no change.

Additional simulations were also performed with a variety of initial conditions. A more realistic initial condition of a 'mid-level' vortex with a weaker surface circulation showed a remarkably similar evolution to the surface vortex case. Genesis did not occur until the inner core had achieved deep near-saturation and the mid-level vortex had elevated, contracted, and intensified. Additional simulations with 'deep' and 'shallow' initial vortex wind fields emphasised the necessity of having both the mid-level vortex and near-saturation in place before genesis could occur, as did simulations with nearly dry soundings (RH = 5%) above z = 7 km and 4 km.

Prior studies have emphasised the role of small-scale vortex formation and merger in the TC genesis process before the time of genesis (Davis and Bosart 2002; Hendricks et al. 2004; Montgomery et. al. 2006). In the simulations presented here, strong, small-scale vertical vorticity anomalies were indeed generated in and around the deep convective towers. For the most part, the processes of their conglomeration were found to be more like 'axisymmetrisation' by the larger, pre-existing circulation and less like vortex merger, except in the cases where an embedded or nearby convective updraught brought the two vortices together by forced low-level convergence (i.e., 'diabatic' vortex merger).

The potential for rapid intensification of the developing and intensifying mid-level vortices was quantitatively measured in terms of the 'kinetic energy efficiency' (KEE), a concept originally defined by Hack and Schubert (1986), and extended to unsteady, nonhydrostatic dynamics by Nolan et al. (2007). It was shown that in the 24 hours before genesis, the KEE more than doubles, and the 'genesis' KEE for the change in the low-level wind field more than triples. These changes shown in Fig. 15 stand in contrast to the usual measures of cyclone intensity, such as maximum surface wind or surface pressure anomaly, which were only very slightly increasing, constant, or even decreasing in the hours before genesis (see e.g., Fig. 1(c), Fig. 11(b)).

Finally, a closer look at the vorticity and diabatic heating fields just before and at the time of genesis showed that the smaller-scale, surface vortex was created by a single, long-lived updraught that erupts very near the centre of the larger mid-level vortex. The trigger for tropical cyclogenesis is the formation of this long-lasting updraught, which organises the low-level vorticity into a single coherent vortex through what might be considered either a repeated or continuous diabatic vortex merger process (Hendricks et al. 2004; Montgomery et al. 2006). However, in these simulations this long-lived updraught does not develop until the thermodynamic and structural changes described above have taken place: near-saturation of the core and increased inertial stability (and efficiency) of the larger-scale, mid-level vortex.

Implications for research and forecasting

While not denying the role of small-scale vortex formation, axisymmetrisation and the occasional merger, the results of this study re-emphasise middle and upper-level saturation and the intensification of a mid-level vortex in the process of tropical cyclogenesis. Indeed, Davis and Bosart (2001) noted that both processes seemed to be at work: they saw that the average, inner-core RH from the surface to 600 hPa approached 95 per cent in the hours before genesis. In this study, we found that near-saturation in the middle levels was necessary to allow for stronger convection to consistently penetrate above the freezing level. The upper-level heating then drove a secondary circulation that intensified the mid-level vortex. This was shown in the time-height diagrams of RH, diabatic heating, and divergence in Fig. 5 and Fig. 9.

Naturally, idealised simulations such as those used in this and the Montgomery et al. (2006) study beg the question of whether or not the genesis process is the same in the real atmosphere. The similarity of these simulations and the *Diana* simulations (Davis and Bosart 2001, 2002; Hendricks et al. 2004), and the observation of a larger, mid-level vortex with embedded vorticity anomalies by airborne Doppler radar (Bister and Emanuel 1997; Reasor et al. 2005) certainly suggest that real genesis events have on occasion followed a similar pathway. The most recent mesoscale modelling study by Davis and Bosart

(2006) of the formation of hurricane *Humberto* (2001) found that in the presence of moderate vertical wind shear, the vorticity of the cyclone built almost entirely upward from the surface, without a stronger mid-level vortex before TC genesis (see their Fig. 10). The very large area over which vorticity was averaged to generate this result, 600 km x 600 km, makes it difficult to rule out that there was some mid-level vortex intensification on the scales seen in our simulations. Li et al. (2006) produced similar time-height diagrams from data averaged over a smaller region (120 km x 120 km) generated by simulations of idealised TC genesis in a monsoon gyre environment; the 15 km resolution of those simulations, however, necessitated cumulus parametrisation which may have biased the divergence toward more convective profiles.

We certainly would not rule out that the genesis process could be different in environments with low to moderate wind shears. The rapid formation and intensification of tropical cyclones, like that of TC *Larry*, is very rarely observed in the presence of significant wind shear (Kaplan and DeMaria 2003). We can speculate that sudden genesis and rapid development is possible when the formation of a nearly saturated, mid-level vortex is allowed by the surrounding environmental conditions. When there is vertical wind shear or other inhibiting factors, perhaps the process is more gradual, with vorticity building upwards from low levels, as also seen by Tory et al. (2006a,b). Idealised WRF simulations of genesis in shear are now underway to explore this issue.

In the North Atlantic basin, the United States government supports airborne reconnaissance of tropical disturbances that have the potential to threaten the US coastline. For disturbances that have not yet been identified as a tropical depression, these aircraft spend much of their time at altitudes as low as 500 m looking for the centre of a low-level circulation. The results of this study suggest that observations of the vertical structure of the wind field and humidity in the disturbance region would also be extremely helpful in evaluating whether TC genesis is imminent. In the cases when a low-level vortex is not readily found, it may be of more use to explore the region at a series of higher altitudes, with dropsondes released at the highest altitudes to more fully sample the moisture field, rather than continuing to criss-cross the area looking for a low-level vortex.

Acknowledgments

The author would like to acknowledge the contributions of David Kofron and Alex Robel in preliminary analyses of the simulations, Eric Rappin for many helpful discussions, and Kerry Emanuel, Daniel Stern, and Yumin Moon for their comments on the manuscript. Computational support for the simulations and data storage was provided by the US National Oceanographic and Atmospheric Administration (NOAA) on the High Performance Computing System at the Geophysical Fluid Dynamics Laboratory (GFDL). This work was supported by NOAA through a grant to the Cooperative Institute for Marine and Atmospheric Science (CIMAS) and by NSF grant ATM-0432551.

References

Australian Bureau of Meteorology 2007. *Severe Tropcial Cyclone Larry*. 24 pp. Available from http://www.bom.gov.au/weather/qld/cyclone/tc_larry/

Bister, M. and Emanuel, K.A. 1997. The genesis of Hurricane Guillermo: TEXMEX analyses and a modeling study. *Mon. Weath. Rev., 125*, 2662-82.

Charney, J.G. and Eliassen, A. 1964. On the growth of the hurricane depression. *J. Atmos. Sci., 21*, 68-75.

Chen, S.S. and Frank, W.M. 1993. A numerical study of the genesis of extratropical convective mesovortices. Part I: Evolution and dynamics. *J. Atmos. Sci., 50*, 2401-26.

Dare, R.A. and Davidson, N.E. 2004. Characteristics of tropical cyclones in the Australian region. *Mon. Weath. Rev., 132*, 3049-65.

Davis, C. and Bosart, L.F. 2001. Numerical simulations of the genesis of Hurricane Diana (1984). Part I: Control simulation. *Mon. Weath. Rev., 130*, 1100-24.

Davis, C. and Bosart, L.F. 2002. Numerical simulations of the genesis of Hurricane Diana (1984). Part II: Sensitivity of track and intensity prediction. *Mon. Weath. Rev., 130*, 1100- 24.

Davis, C.A. and Bosart, L.F. 2006. The formation of Hurricane Humberto (2001): The importance of extratropical precursors. *Q. Jl R. Met. Soc., 132*, 2055-85.

Eliassen, A. 1951. Slow thermally or frictionally controlled meridional circulation in a circular vortex. *Astrophys. Norv., 5*, 19-60.

Emanuel, K.A. 1989. The finite-amplitude nature of tropical cyclogenesis. *J. Atmos. Sci., 46*, 3431-56.

Emanuel, K.A. 2005. Genesis and maintenance of "Mediterranean hurricanes." *Advances in Geosciences, 2*, 217-20.

Frank, W.M. 1987. *Tropical cylone formation. A Global View of Tropical Cyclones*. R. Elsberry et al. (eds). Naval Postgraduate School, Monterey, CA.

Fritsch, J.M., Murphy, J.D. and Kain, J.S. 1994. Warm core vortex amplification over land. *J. Atmos. Sci., 51*, 1780-807.

Gray, W.M. 1968. Global view of the origins of tropical cyclones. *Mon. Weath., Rev., 96*, 669-700.

Hack, J.J. and Schubert, W.H. 1986. Nonlinear response of atmospheric vortices to heating by organized cumulus convection. *J. Atmos. Sci., 43*, 1559-73.

Hendricks, E.A., Montgomery, M.T. and Davis, C.A. 2004. The role of "vortical" hot towers in the formation of Tropical Cyclone Diana (1984). *J. Atmos. Sci., 61*, 1209-32.

Hong, S.-Y., Dudhia, J. and Chen, S.-H. 2004. A revised approach to ice microphysical processes for the parameterization of clouds and precipitation. *Mon. Weath. Rev., 132,* 103-20.

Hong, S.-Y. and Pan, H.-L. 1996. Nonlocal boundary layer vertical diffusion in a medium-range forecast model. *Mon. Weath. Rev., 124*, 2322-39.

Houze, R.A. 1997. Stratiform precipitation in regions of convection: a meteorological paradox? *Bull. Am. Met. Soc., 78*, 2179–96.

Jordan, C.L. 1958. Mean soundings for the West Indies area. *J. Met., 15*, 91-7.

Kaplan, J. and DeMaria, M. 2003. Large-scale characteristics of rapidly intensifying tropical cyclones in the North Atlantic basin. *Weath. forecasting, 18*, 1093-108.

Laprise, R. 1992. The Euler equations of motion with hydrostatic pressure as an independent variable. *Mon. Weath. Rev., 120*,197-207.

Li, Tim, Ge, X., Wang, B. and Zhu, Y. 2006. Tropical cyclogenesis associated with Rossby wave energy dispersion of a pre-existing typhoon. Part II: Numerical simulations. *J. Atmos. Sci., 63*, 1390-409.

McBride, J.L. 1981. Observational analysis of tropical cyclone formation. Part I: Basic definition of data sets. *J. Atmos. Sci., 38*, 1117-31.

McBride, J.L. and Zehr, R. 1981. Observational analysis of tropical cyclone formation. Part II: Comparison of non-developing versus developing systems. *J. Atmos. Sci., 38,* 1132-51.

Malkus, J.S. and Riehl, H. 1960. On the dynamics and energy transformations in steady-state hurricanes. *Tellus, 12*, 1-20.

Mapes, B.E. and Houze Jr., R.A. 1995. Diabatic divergence profiles in western Pacific mesoscale convective systems. *J. Atmos. Sci., 52*, 1807–28.

Montgomery, M.T., Nicholls, M.E., Cram, T.A. and Saunders, A.B. 2006. A vortical hot tower route to tropical cyclogenesis. *J. Atmos. Sci., 63*, 355-86.

Noh, Y., Cheon, W.-G., Hong, S.-Y. and Raasch, S. 2003. Improvement of the K-profile model for the planetary boundary layer based on large eddy simulation data. *Bound. Lay. Met., 107*, 401-27.

Nolan, D.S. and Grasso, L.D. 2003. Nonhydrostatic, three-dimensional perturbations to balanced, hurricane-like vortices. Part II: Symmetric response and nonlinear simulations. *J. Atmos. Sci., 60*, 2717-45.

Nolan, D.S., Montgomery, M.T. and Grasso, L.D. 2001. The wavenumber-one instability and trochoidal motion of huricane-like vortices. *J. Atmos. Sci., 58*, 3243-70.

Nolan, D.S. and Montgomery, M.T. 2002. Nonhydrostatic, three-dimensional perturbations to balanced, hurricane-like vortices. Part I: Linearized formulation, stability, and evolution. *J. Atmos. Sci., 59*, 2989-3020.

Nolan, D.S., Moon, Y. and Stern, D.P. 2007. Tropical cyclone intensification from asymmetric convection: Energetics and efficiency. *J. Atmos. Sci., 64*, 3377-405.

Ooyama, K. 1964. A dynamical model for the study of tropical cyclone development. *Geofys. Int., 4*, 187-98.

Ooyama, K. 1969. Numerical simulation of the life cycle of tropical cyclones. *J. Atmos. Sci., 26*, 3-40.

Raymond, D. and Jiang, H. 1990. A theory for long-lived mesoscale convective systems. *J. Atmos. Sci., 47,* 3067-77.

Raymond, D.J., Lopez-Carrillo, C. and Cavazos, L.L. 1998. Case studies of developing East Pacific easterly waves. *Q. Jl R. Met. Soc., 124*, 2005-34.

Reasor, P.D., Montgomery, M.T. and Bosart, L.F. 2005. Mesoscale observations of the genesis of Hurricane Dolly (1996). *J. Atmos. Sci., 62*, 3151-71.

Riehl, H. and Malkus, J.S. 1961. Some aspects of Hurricane Daisy, 1958. *Tellus, 13*, 181-213.

Ritchie, E.A. and Holland, G.J. 1997. Scale interactions during the formation of Typhoon Irving. *Mon. Weath. Rev., 125*, 1377–96.

Rogers, R., Black, M.L., Chen, S.S. and Black, R.A. 2007. An evaluation of microphysical fields from mesoscale model simulations of tropical cyclones. Part I: Comparisons with observations. *J. Atmos. Sci., 64,* 1811-34.

Rotunno, R. and Emanuel, K.A. 1987. An air-sea interaction theory for tropical cyclones. Part II: Evolutionary study using a nonhydrostatic axisymmetric mumerical model. *J. Atmos. Sci., 44*, 542-61.

Schubert, W.H. and Hack, J.J. 1982. Inertial stability and tropical cyclone development. *J. Atmos. Sci., 39*, 1687-97.

Simpson, J., Ritchie, E., Holland, G.J. Halverson, J. and Stewart, S. 1997. Mesoscale interactions in tropical cyclone genesis. *Mon. Weath. Rev., 125*, 2643-61.

Sippel, J.A., Nielsen-Gammon, J.W. and Allen, S.E. 2006. The multiple-vortex nature of tropical cyclogenesis. *Mon. Weath. Rev., 134,* 1796-814.

Skamarock, W.C., Klemp, J.B., Dudhia, J., Gill, D.O., Barker, D.M., Wang, W. and Powers, J.G. 2005. A Description of the Advanced Research WRF Version 2. *NCAR technical note 468+STR*, 88 pp.

Tory, K.J., Montgomery, M.T. and Davidson, N.E. 2006a. Prediction and diagnosis of tropical cyclone formation in an NWP system. Part I: The critical role of vortex enhancement in deep convection. *J. Atmos. Sci., 63*, 3077-90.

Tory, K.J., Montgomery, M.T. and Davidson, N.E. 2007. Prediction and diagnosis of tropical cyclone formation in an NWP system. Part III: Developing and non-developing storms. *J. Atmos. Sci., 64,* 3195-213.

Tory, K.J., Montgomery, M.T., Davidson, N.E. and Kepert, J.D. 2006b. Prediction and diagnosis of tropical cyclone formation in an NWP system. Part II: A diagnosis of tropical cyclone Chris formation. *J. Atmos. Sci., 63*, 3091-113.

Wicker, L.J. and Skamarock, W.C. 2002. Time-splitting methods for elastic models using forward time schemes. *Mon. Weath. Rev., 130,* 2088-97.

Yuter, S.E. and Houze Jr, R.A. 1994. Three-dimensional kinematic and microphysical evolution of Florida cumulonimbus. Part III: Vertical mass transport, mass divergence, and synthesis. *Mon. Weath. Rev., 123*, 1964-83.

Zehr, R. 1992. Tropical cyclogenesis in the Western North Pacific. *NOAA Tech. Rep., NESDIS 61*, 181 pp.